UCHL1 inhibited by A1 astrocytes facilitates aggregates clearance to promote neural stem cells activation after spinal cord injury

Lu Ding[1,6], Weiwei Chu[1,2,6], Yu Xia[1], Tian Li[3], Ming Shi[1], Feng-Quan Zhou[4,5,*], David Y.B. Deng[1,7,*]

[1]Scientific Research Center, The Seventh Affiliated Hospital, Sun Yat-sen University, Shenzhen 518107, China

[2]School of Pharmaceutical Sciences (Shenzhen), Sun Yat-sen University, Shenzhen 518107, China

[3]Obstetrics and Gynecology Department, The Seventh Affiliated Hospital, Sun Yat-sen University, Shenzhen 518107, China

[4]Department of Orthopaedic Surgery, Johns Hopkins University School of Medicine, Baltimore, Maryland 21287, USA

[5]The Solomon H. Snyder Department of Neuroscience, Johns Hopkins University School of Medicine, Baltimore, Maryland 21287, USA

[6]These authors contributed equally

[7]Lead contact

*Correspondence: dengyub@mail.sysu.edu.cn (D.-Y.B.D.); fzhou4@jhmi.edu (F.-Q.Z.)

Abstract

Spinal cord injury (SCI) is a devastating central nervous system (CNS) disease with no satisfying therapies available. Mobilizing endogenous neural stem cells (NSCs) to trigger intrinsic regeneration exhibits promising potentials for SCI repair. However, neurogenesis from endogenous NSCs is extremely restricted in the non-neurogenic spinal cord after SCI. Accumulation of protein aggregates has been shown to impede quiescent NSCs activation and the subsequent neurogenesis. Here, we found that ubiquitin c-terminal hydrolase l-1 (UCHL1), a deubiquitinating enzyme, functioned to regulate NSCs activation and neurogenesis by reducing protein aggregations through ubiquitin-proteasome pathway (UPP) in vitro. Upregulation of UCHL1 in spinal cord NSCs of rats with complete transection SCI efficiently enhanced NSCs proliferation and neurogenesis, leading to significantly improved functional outcomes. Based on protein microarray analysis of cerebrospinal fluid (CSF), our results revealed that A1 reactive astrocytes acted to restrict NSCs neurogenesis by negatively regulating UCHL1-depentdent protein aggregates removal via the C3/Nrf2 signaling. Indeed, blockade of A1 astrocytes using neutralizing antibodies after SCI also led to NSCs activation, increased neurogenesis and remarkably enhanced motor function recovery. This study not only revealed a novel mechanism regulating NSCs-medicated neurogenesis in the spinal cord, but also provided new molecular targets for neural repair strategies after SCI.

INTRODUCTION

Spinal cord injury (SCI) is an overwhelming neurotraumatic disease typically resulting in permanent disability, for which no curative therapy is available [1]. However recently neurorestorative treatments have been able to partially restore the damaged neurological functions due to SCI [2, 3]. Existent of endogenous neural stem cells (NSCs) in the adult spinal cord provides an potential approach for spinal cord repair after SCI, with benefits of circumventing several risks and limitations of stem cell transplantation therapy [4, 5]. Unfortunately, neurogenesis from endogenous NSCs is extremely limited in the adult spinal cord in vivo, despite their inherent plasticity to proliferate and give rise to neurons in vitro [6-8]. Such non-neurogenic feature of injured spinal cord in vivo suggests the presence of negative influences from the spinal cord microenvironment on NSCs. Therefore, elucidating the mechanisms by which spinal cord microenvironment regulates endogenous NSCs-mediated neurogenesis is of great importance for enhancing spinal cord regeneration after SCI. Indeed, emerging evidences have demonstrated that endogenous NSCs could be mobilized to generate neurons for SCI repair through in vivo reprogramming, supplement of growth facilitator, or targeted intervention et. al. [9-12].

Maintance of protein homeostasis is vital for the proper cell function over the long lifetime. Imbalance of proteostasis results in accumulation of misfolded and unwanted proteins, which is associated with stem cell

dysfunction, aging and neurodegenerative disorders [13]. Ubiquitin-proteasome system (UPS), a major intracellular protein degradation system, is one of the primary mechanisms to maintain proteostasis. Recent transcriptomic analysis reported that protein aggregates clearance mediated by lysosomes/proteasome played critical roles in regulation of NSC activation. Specifically, in aged mouse brains quiescent NSCs have reduced activation capacity due to lysosome defects and accumulation of protein aggregates, whereas enhancing lysosome function restored their ability to be activated [14]. Similarly, Morrow et al. found that adult quiescent NSCs could rely on vimentin-mediated proteasome localization to the aggresome to clear proteins during activation. In contrast, knocking out vimentin in NSCs impaired proteostasis recovery and delayed quiescence exit [15], suggesting the potentially pivotal role of UPS in NSC activation.

Ubiquitin C-terminal Hydrolase L1 (UCHL1) is an abundant deubiquitinating enzyme indispensable for proper UPS function that selectively expresses in neurons [16, 17]. Previous studies have shown that UCHL1 is functionally involved in neurodegenerative diseases, likely through its function to clear abnormal protein aggregates [17-19]. For instance, upregulation of UCHL1 improved synaptic function and contextual memory by decreasing β-amyloid formation in Alzheimer's disease (AD) [16, 20]. UCHL1 could also preserve axonal conductance and improve motor behavior after stroke [21]. Moreover, UPS and the ubiquitin levels are also essential for the neural

regeneration, development and differentiation of neural stem and progenitor cells after SCI [22, 23]. In light of its favorable ability in clearing protein aggregations, it is likely that UCHL1 might contribute to the spinal cord microenvironment hampering endogenous NSCs activation and neurogenesis after SCI. The pathological milieu of spinal cord is a vital factor controlling proteasome functions and might underlie the alternative non-neuronal fate of endogenous NSCs after SCI. In support, higher levels of UCHL1 in spinal cord interneurons have been correlated with their increased survival after SCI [23, 24]. In contrast, failure to upregulate UPS activity in motor neurons after SCI might undermine their ability to survive and recover.

Local astrocyte populations play an important role in creation of a neurogenic environment, which not only maintains various homeostatic functions of central nervous system (CNS), but also prevents inflammatory transitions after acute insults like stroke and SCI [25, 26]. Although it is still controversial regarding the classification and contribution of reactive astrocytes to CNS diseases and repair [27], increasing evidence has reported a new subtype of A1 reactive astrocytes that act in a neurotoxic manner to kill neurons and oligodendrocytes [28, 29]. Reduction of A1 reactive astrocytes protected axotomized neurons and improved functional performance after acute SCI [30-32]. A1 astrocytes remarkably upregulate many classical complement cascade genes, with the highest level of C3. C3-expressing A1 astrocytes have been implicated in multiple neurodegeneration disorders that

share the common feature of accumulating neurotoxic proteins in neurons [28]. Blockade of C3 rescued synaptic loss and cognitive decline caused by β-amyloid (Aβ) oligomers and tau pathology in AD/PD animal models [33, 34]. Therefore, as one of the most abundant cells in the spinal cord, it is possible that A1 astrocytes in some way participate in regulation of UCHL1-mediated protein aggregations clearance in endogenous NSCs post-SCI.

Here, we explored the potential effects of A1 astrocytes and UCHL1-mediated protein aggregates clearance on spinal cord NSC activation and neurogenesis following SCI. Our results showed that the level of UCHL1 decreased after SCI and its upregulation facilitated NSC proliferation and neuronal differentiation by eliminating protein aggregations through ubiquitin-proteasome pathway (UPP). Based on protein microarray analysis of cerebrospinal fluid (CSF), we further revealed that A1 astrocytes activated by SCI acted to inhibit UCHL1 and UPP by C3 production, resulting in protein aggregates accumulation in endogenous NSCs and reduced NSC activation. Functionally, either overexpression of UCHL1 or inhibition of A1 astrocyte formation after SCI enhanced NSC-derived neurogenesis and motor function recovery. Together, our present study demonstrated that A1 reactive astrocytes hindered the potential capacity of endogenous NSCs for neurogenesis after SCI by repressing UCHL1-mediated proteasome function, thus providing novel molecular targets for future stem cell-based therapy of CNS disorders.

RESULTS

UCHL1 level in the spinal cord was significantly down regulated after SCI

CNS damage generally causes dysfunctions of UPP, resulting in depletion of free ubiquitin and increased ubiquitinated proteins. We therefore investigated the ubiquitin C-terminal hydrolases (UCHL1, UCHL3, UCHL5) that act to maintain free ubiquitin level and proper UPS function. Results showed that UCHL1, a neuron-specific isoform, was strongly detected in the brain and the spinal cord, compared with 2 other isoforms UCHL3 and UCHL5 (Figures 1A-1C). At 24 hours after SCI a remarkable down-regulation of UCHL1 levels was observed in the gray matter (Figure 1D), and it dramatically decreased within three days post-injury (Figures 1E and 1F). Further immunofluorescent staining showed that UCHL1 positive cells did not overlap with $NG2^+$ Oligodendrogenic progenitor cells or $GFAP^+$ astrocytes (Figure 1G). Instead, they were specifically enriched not only in the spinal neurons ($NeuN^+$) (Figure 1G), but also co-localized with $Nestin^+$ cells, a specific marker for spinal cord endogenous NSCs [35-37]. The level of UCHL1 was remarkably decreased in NSCs after SCI (Figures 1H and 1I), suggesting that it might be involved in SCI-induced biological process of spinal cord NSCs.

UCHL1 promoted NSCs proliferation and neuronal differentiation by accelerating removal of protein aggregates through UPP

Emerging evidence has suggested a significant difference of protein

aggregates and UPS activity between the activated and quiescent NSCs [14]. To explore whether UCHL1 was involved in the protein aggregates within NSCs, NSCs extracted from the brain of fetal rats were utilized due to the limited endogenous NSCs in spinal cord. Cells were infected with either empty lentiviral vector (NC-LV), lentiviral vector encoding UCHL1 (OE-UCHL1-LV), or treated with LDN-57444, an effective inhibitor of UCHL1 [18]. QPCR (Figure 2A) and Western blot analyses (Figures 2B and 2C) confirmed the successful overexpression of UCHL1 in NSCs at 48 hours after infection. To label the intracellular aggregations, we used Proteostat dye, which exhibited brightly red fluorescent when binds to denatured protein cargo with aggresome and aggresome-like inclusion bodies. As shown in Figures 2D-2F, many protein aggregates were accumulated in the control NSCs, while NSCs infected with OE-UCHL1-LV had significantly less Proteostat staining. In contrast, the UCHL1 inhibitor LDN-57444 treatment resulted in more abundance of aggregates than that of the control. Moreover, it also reversed the decreased protein aggregates in NSCs with UCHL1 overexpression (Figures 2D-2F). No difference was observed between the control and NC-LV group, indicating lentiviral vector *per se* had no effect. In addition, flow cytometry assay also revealed that overexpression of UCHL1 led to protein aggregations elimination in NSCs, whereas increased protein aggregations were detected when UCHL1 was blocked by LDN-57444 (Extended Data Figures 1A and 1B).

A recent study reported that increased protein aggregates accumulation

in quiescent NSCs reduced their ability to be activated [14]. Thus, we examined whether UCHL1 regulated the proliferation of NSCs using EdU incorporation assay. Immunofluorescent staining (Figures 2G and 2H) and flow cytometry analysis (Extended Data Figures 1C and 1D) both showed that UCHL1 overexpression (OE-UCHL1-LV) in NSCs resulted in elevated number of EdU^+ cells, which was abolished by LDN-57444 treatment. Furthermore, up-regulation of UCHL1 in NSCs led to more Tubulin β3+ neurons, whereas NSCs treated with LDN-57444 mainly differentiated into astrocytes (Extended Data Figures 2A and 2B). In addition to neurons, the number of CNPase positive oligodendrocytes was also slightly increased in the OE-UCHL1-LV group (Extended Data Figures 2A and 2B). These results suggested that increased level of UCHL1 in NSCs might facilitate their proliferation and neuronal differentiation by accelerating the clearance of intracellular protein aggregates.

To test this hypothesis, we first examined if manipulation of protein aggregates in NSCs could affect their activation. Because nutrient deprivation has been shown to significantly decrease protein aggregates in NSCs [14], we incubated NSCs in HBSS prior to be treated with activation factors epidermal growth factor (EGF) and fibroblast growth factor (FGF). The results showed that nutrient deprivation depleted protein aggregations in NSCs (Extended Data Figures 3A-3D) and enhanced NSC activation in response to growth factors (Extended Data Figures 3E-3H). In contrast, administration of MG132,

a proteasome inhibitor, resulted in accumulation of protein aggregates within NSCs (Extended Data Figures 3A-3D) and remarkably decreased cell proliferation (Extended Data Figures 3E-3H). To further determine if UCHL1 activated NSCs by clearing protein aggregates through UPP, we monitored the proteasome activity using the proteasome-specific affinity probe. Flow cytometry assay revealed that compared with the control or the empty lentiviral vector group, NSCs in the OE-UCHL1-LV group had increased proteasome activity (Figures 2I and 2J). Conversely, NSCs treated with UCHL1 inhibitor LDN-57444 or the proteasome inhibitor MG132 led to significantly reduced level of proteasome activities (Figures 2I and 2J). Consistently, western blot analysis demonstrated that UCHL1 overexpression increased the expression level of proteasome 20S, whereas LDN57444 or MG132 treatment had the opposite effect (Figures 2K and 2L). Together, these data provided strong evidence that UCHL1 could activate endogenous NSCs to proliferate and give rise to neurons, likely due to its positive effect on the protein aggresome clearance through UPS.

C3 induced accumulation of intracellular protein aggregation via the C3/Nrf2 pathway to impede NSCs activation

How does SCI lead to reduced UCHL1 level and failed activation of endogenous NSCs? CSF is well known for its role as a circulating media containing signaling molecules regulating important CNS functions. Thus, we

used protein microarray analysis to compare a spectrum of cytokines in CSF before and after SCI. From the hierarchical clustering analysis, 52 of total 88 cytokines were significantly upregulated after SCI, among which 26 showed more than 2-fold changes (Figure 3A). KEGG analysis revealed that the significantly altered cytokines were mainly linked to signaling pathways associated with immune-inflammation responses, such as the complement and coagulation cascades, TNF and NFκB signaling pathways, etc. (Figure 3B). Interestingly, the levels of several astrocyte-related factors, including C3, GFAP, S100B and S100A were all markedly increased in CSF after SCI (Figure 3A).

As part of the innate immune system, the complement system in the CNS is emerging to be important factor mediating the crosstalk between different cell types during development or after injury. For instance, complement factor C3 has been shown to be activated in AD brain and involved in neurodegeneration processes [33, 34]. We therefore tested if C3 was involved in the presence of excessive protein aggregations resistant to proteolysis in NSCs. First, ELISA assays were used to measure the levels of C3a in the CSF or serum samples from normal or SCI animals. Data revealed that the level of C3a was obviously increased in the CSF of SCI rats at 6 hours after injury (Extended Data Figure 4A). Similarly, the level of C3a was also elevated in the serum from three days to three weeks after SCI (Extended Data Figure 4B). Moreover, elevated leve of C3 was also detected in the spinal

tissues during the acute phase after SCI (Figures 3C-3F). Second, to investigate the functional influence of C3 on protein aggregation in NSCs, we examined if NSCs express C3a receptor (C3aR). Results showed presence of C3aR in the cytomembrane of NSCs, similar to that in BV2 microglia expressing high level C3aR (Figures 3G and 3H). NSCs were incubated with C3 for 24 hours in vitro, followed by the evaluation of aggresome formation and cell proliferation. The results showed that accumulation of protein aggregations was significantly increased in NSCs treated with C3 in a dose-dependent manner (Figures 3I and 3J; Extended Data Figures 4C and 4D). In support, flow cytometry analysis also demonstrated that C3 administration could inhibit proteasome activity in NSCs (Figures 3K and 3L). Third, by using Edu assay we found that C3 treatment led to significant reduction of NSC proliferation (Figures 3M and 3N; Extended Data Figures 4E and 4F), correlating with increased protein aggregates.

We next investigated how C3 affected the level of UCHL1 and related regulatory pathways. Imbalance of oxidant stress responses usually result in increased level of toxic aggresome [24]. Reactive oxygen species (ROS) and Nrf2 are the key pro-oxidant and anti-oxidant regulators, The increased production of proteasome 20S contributes to enhanced Nrf2-depedent cellular ability to degrade oxidized proteins [38]. Here we found that C3 treatment resulted in the decreased expression levels of UCHL1, ubiquitin and Nrf2 (Figures 3O and 3P). Moreover, ROS inhibitor or C3aR inhibitor treatment

obviously rescued UCHL1 expression (Extended Data Figures 4G and 4H), suggesting C3/ROS/Nrf2 signaling might be involved in protein aggregates degradation. These results taken together suggest that C3 could suppress endogenous NSC activation by inhibiting UCHL1 and proteasome activity via the ROS/Nrf2 pathway to slow down the degradation of protein aggregates.

A1 reactive astrocytes suppressed NSC activation and neuronal differentiation by secreting C3 to inhibit aggresome elimination

It has been reported that C3 is one of the typical and abundantly expressed biomarkers in A1 reactive astrocytes [28, 33]. Thus we proposed that acute insult to spinal cord tissues would lead to activation of A1 astrocytes, which in turn secret C3 to diminish abnormal protein aggregates removal in NSCs. To test this idea, we used purified astrocytes to produce A1 phenotype with three cytokines, TNFα/IL-1α/C1q, as previously described [28]. High level expression of C3 indicated the successful induction of A1 astrocytes (Figures 4A-4D). Next, control and A1 astrocytes or their condition media (ACM) were co-cultured with NSCs, respectively (Figure 4E). After 24 hours, A1 astrocytes or their ACM, but not the control astrocytes or their ACM, resulted in a mass deposition of aggresome in the cytoplasm of NSCs (Figures 4F and 4G; Extended Data Figures 5A and 5B). On the other hand, the proliferating capacity of NSCs treated with A1 astrocytes or their ACM were significantly diminished, whereas control astrocytes or their ACM treatment had no effect

(Figures 4H and 4I; Extended Data Figures 5C and 5D). Consistently, flow cytometry data showed that proteasome activity was reduced by A1 astrocytes or their ACM (Figures 4J and 4K), which was further confirmed by the decreased level of proteasome 20S or UCHL1 (Figures 4L and 4M). Furthermore, up-regulation of C3 and reduced level of Nrf2 were detected in NSCs cultured with A1 astrocytes/ACM (Figures 4N and 4O). To further confirm the connection among A1 astrocytes, C3 and NSCs' response, NSCs were overexpressed with UCHL1 or treated with C3aR inhibitor in the context of A1 reactive astrocytes conditioned medium (A1 ACM). Western blot analysis revealed that the expression of UCHL1, ubiquitin and proteasome 20s activity were all rescued by UCHL1 overexpression and/or C3aR blockade in NSCs cultured with A1 ACM (Extended Data Figures 5E and 5F). These data implicated that A1 astrocytes could inhibit NSC activation by inhibiting the function of proteasome to clear aggresome via C3/Nrf2 pathway.

Complement pathway and A1 astrocytes play critical role in synaptic toxicity and neuronal degenerative process [33]. Here we found that compared to NSCs with no treatment, NSCs co-cultured with control astrocytes or their ACM differentiated into neurons and extended long processes (Extended Data Figures 6A and 6B). In contrast, NSCs co-cultured with A1 astrocytes or their ACM had very short processes (Extended Data Figures 6A and 6B). To further assess the effects of A1 astrocytes on NSCs differentiation and neurite growth, immunofluorescence staining with neuronal marker doublecortin (DCX)

showed higher proportion of DCX$^+$ neurons with longer processes from NSCs co-cultured with control astrocytes or their ACM compared with those co-cultured with A1 astrocytes or their ACM (Extended Data Figures 6C-6E). In contrast, NSCs co-cultured with A1 astrocytes or their ACM produced more GFAP positive astrocytes (Extended Data Figures 6C and 6D). In addition, a mild decreased number of CNPase$^+$ oligodendrocytes were also observed in A1 astrocytes/ACM treatment compared to other groups (Extended Data Figures 6C and 6D). Together, these results suggested that A1 astrocytes suppressed the neuronal differentiation of NSCs and the subsequent neurite extension.

Up-regulation of UCHL1 enabled endogenous NSC activation and neuronal differentiation in rat spinal cord after SCI

NSCs usually keep low proliferation and self-renew rate in the normal CNS, but they show potential to proliferate and give rise to neurons under trauma condition. However, the activation of NSCs in response to SCI is not enough, and very few neurons can be generated under the inhibitory injury microenvironment. NSCs extracted from the fetal brain of embryonic day 14 SD rats could form neurospheres and express both of Nestin and SOX2 (two typical stem cell markers) in vitro (Extended Data Figure 7A). Compared with the intact spinal cord, the number of Nestin/SOX2$^+$ cells were increased near the lesion location at 5-day after SCI, which also exhibited shape

transformation with hypertrophy and thickening process (Extended Data Figure 7B). Moreover, a higher rate of Ki-67/Nestin$^+$ cells were observed after SCI (Extended Data Figures 7C and 7D), and approximately 79.83% SOX2$^+$ cells were Nestin/SOX2$^+$ cells (Extended Data Figure 7D), suggesting that most of the Nestin$^+$ cells might be endogenous NSCs and could be activated by SCI.

To determine the potential effects of UCHL1 on endogenous spinal cord NSC activation in vivo, the T10 spinal cord transection rat model was used. To manipulate UCHL1 level in the spinal cord, lentiviral vector encoding UCHL1 (OE-UCHL1-LV), recombinant human UCHL1 protein (rh-UCHL1), or specific UCHL1 inhibitor LDN-57444 was injected into the injury site. Spinal cord tissues containing the injured center were extracted at 7 days post-SCI to evaluate the expression of UCHL1. Western blotting analysis showed that the level of endogenous UCHL1 was significantly reduced after SCI, whereas OE-UCHL1-LV or rh-UCHL1 treatment restored its level (Figures 5A and 5B). In addition, the protein level of proteasome 20S was also elevated, implying enhanced UPS activity with higher UCHL1 level (Figures 5A and 5B). To detect the distribution of OE-UCHL1-LV infected cells in vivo, GFP positive cells around the lesion center of spinal cord were quantified at 5 days after SCI. Approximately 82.91% GFP$^+$ (lenti-viral infected cells) were Nestin$^+$ cells, and a few NG2$^+$ oligodendrogenic progenitor cells (9.27%) and Tubulin β3$^+$ neurons (5.41%) were also GFP$^+$. In contrast, very few NeuN$^+$ neurons or

GFAP$^+$ astrocytes were GFP$^+$, indicating the high infection efficiency and specificity of lentiviral vectors in Nestin$^+$ NSCs in the spinal cord in vivo (Figures 5C and 5D).

We next examined the recruitment and activation of NSCs at the spinal cord injury site. Double immunofluorescent staining for Nestin and GFAP showed that under control or empty viral vector treatment (NC-LV), the number of Nestin$^+$ cells at the injury site were relatively low (Figures 5E-5F). In contrast, increasing levels of UCHL1 with either lenti-viral mediated overexpression or recombinant protein treatment significantly elevated the number of Nestin$^+$ cells at the injury site (Figures 5E-5F). Conversely LDN-57444 treatment led to fewer Nestin$^+$ cells (Figures 5E-5F). In addition to the changes in Nestin$^+$ cells, the results also showed that increasing UCHL1 level better preserved the tissue integrity with smaller cavities at the injury site (Figure 5G). Together, these results suggest that UCHL1 act to promote the accumulation or proliferation of Nestin$^+$ cells at the spinal cord lesion site.

Co-labeling of Ki-67 and Nestin$^+$ cells within the lesion core were performed to evaluate endogenous NSC proliferation. OE-UCHL1-LV or rh-UCHL1 treatment led to obviously increased level of Ki-67/Nestin$^+$ cells (Figures 6A and 6B), whereas LDN-57444 reduced their level (Figures 6A and 6B), indicating that UCHL1 functioned to promote spinal NSC proliferation after SCI. Moreover, increased number of β3 Tubulin$^+$ mature neurons were also detected in rats treated with OE-UCHL1-LV or rh-UCHL1 (Figures 6C and 6E),

indicating increased number of neurons. Some of these neurons were co-labeled with GFP in animals infected with OE-UCHL1-LV (Figure 6D), suggesting that they might be differentiated from endogenous NSCs. Collectively, these results implicated that UCHL1 could facilitate endogenous NSC proliferation and neuronal differentiation in vivo, likely through enhanced UPS activity.

Overexpression of UCHL1 promoted nerve regeneration and functional recovery after SCI

To investigate how UCHL1-induced NSC activation affect neuronal recovery after SCI, the injured spinal cord segments were dissected out and sectioned at 8 weeks after the injury. Anatomical analysis displayed that administration of OE-UCHL1-LV or rh-UCHL1 significantly promoted the tissue integrity at the lesion site, while larger tissue defects were observed in other treatments (Figure 7A; Extended Data Figure 8A). The spinal cord tissue sections were also stained with the axonal marker NF-200. Significantly increased numbers of axons were observed at the damage epicenter in OE-UCHL1-LV or rh-UCHL1 group (Figures 7A-7B). In contrast, very few NF-200 positive axons were detected in two controls or LDN-57444 treated samples (Figures 7A-7B). Previous studies demonstrated that SCI often resulted in drastically reduced 5HT positive fibers below the injury site. In consistent, remarkable loss of 5HT positive fiber was observed in the lesion

center of control animals (Extended Data Figure 9). As expected, replenishment of UCHL1 seemed to have more $5HT^+$ fibers detected entering the injury site in the OE-UCHL1-LV or rh-UCHL1 treated rats (Extended Data Figure 9).

To determine whether enhanced axonal regrowth, presumably from endogenous NSCs activation by UCHL1 physiological functional recovery post-lesion, motor behavioral outcomes were assessed weekly by BBB score test. Severe hindlimb locomotion deficits were observed in all groups during the first four weeks after SCI (Figure 7C). Rats treated with OE-UCHL1-LV or rh-UCHL1 exhibited significant improvement of BBB scores from the 5th week post-injury, which reached a plateau at the 8th week post-surgery (Figure 7C). No significant differences were found between the lesion control and NC-LV animals. As expected, blocking UCHL1 activity with LDN-57444 impaired the spontaneous recovery of hind limbs (Figure 7C). The representative behavior of the hindlimbs' motion was illustrated in Extended Data Figure 8B. To confirm the dependance of locomotor restoration on axonal sprouting into the lesion center, electrophysiological assay was performed before perfusion. A stimulating electrode was positioned intraspinally at the dorsal T7 spinal cord (3 segments above the lesion), and any evoked activity at T13 spinal cord (3 segments below the lesion) was recorded (Figure 7D). In the uninjured animals, a short latency response was evoked by stimulation at T7, which was entirely abolished after T10 transection (Figures 7E and 7F). After 8 weeks, evoked

response was partially restored in injured animals treated with OE-UCHL1-LV or rh-UCHL1, implying the formation of synaptic relays in the lesion epicenter. Although smaller than the intact animals, response amplitudes in OE-UCHL1-LV or rh-UCHL1 group were significantly higher than that of the controls (Figures 7E and 7F). These data suggested that activation of NSCs by UCHL1 improve neural circuit reconstruction at the injury site and restore neuroelectric circuit conductivity, therefore contributing to locomotor functional recovery after SCI.

Block of A1 astrocytes using neutralizing antibodies effectively enhanced endogenous regenerative ability and motor functional recovery following SCI

Based on above results, it raised the possibility that blockade of A1 astrocytes might activate NSCs by regulating the C3/UCHL1 pathway in vivo. Previous research has demonstrated that administration of neutralizing antibodies against Il-1α, TNFα, and C1q together could successfully inhibit A1 astrocyte formation [28]. Given the dosage of neutralizing antibodies，BALB/C mice SCI model was used and neutralizing antibodies against IL-1α, TNFα and C1q was injected intraperitoneally weekly (Figure 8A). SCI rapidly induced massive A1 astrocytes generation at acute phase (7 days after injury), and neutralizing antibodies, but not the IgG isotype control, successfully blocked A1 astrocyte formation (Figures 8B and 8C). Some NSCs could be activated

by SCI, and much more Nestin/SOX2^{+} NSCs were observed in neutralizing antibody treated animals (Figures 8D and 8E). Notably, many NSCs around the central canal and near the lesion epicenter were strongly stimulated to proliferate by neutralizing antibody administration (Figures 8F-8G). Western blotting analysis confirmed the decreased levels of C3 after blockade of A1 astrocytes, as well as the increased levels of UCHL1 and proteasome 20S (Figures 8H-8I). No significant difference was detected between the lesion control and IgG groups. Our data implied that A1 astrocyte inhibition contributed to NSC activation post-SCI, likely through the C3/UCHL1 pathway.

To evaluate whether activated NSCs could migrate into the injury site with astrocyte-modified microenvironment, mice were sacrificed at 6-week after injury. Immunofluorescence staining showed obvious accumulation of Nestin^{+} NSCs surrounding and inside the injury site in animals treated with neutralizing antibodies, whereas Nestin^{+} cells in the control or IgG group were mostly surrounded the lesion borders, rarely in the epicenter (Extended Data Figure 10A), indicating that A1 blockade effectively enhanced NSC migration into the injury site. Moreover, a higher proportion of β3 Tubulin^{+} neurons in and around the lesion center was observed after A1 astrocytes suppression (Extended Data Figure 10A). Furthermore, in the neutralizing antibody treated animals, NSCs were observed to be intermingled with NeuN^{+} neurons beyond the lesion borders, and some of them formed terminal-like structure with contacted neurons (Extended Data Figure 10B), implying the interactions

between NSCs-derived neurons with old residential neurons. Therefore, blocking A1 astrocytes efficiently enhanced NSC recruitment inside the lesion site and might partially give rise to neurons after SCI.

Axonal regeneration was next assessed by labeling axons that grew into lesion site or beyond with NF-200. Importantly, in animals treated with neutralizing antibodies, dense bundles of axons extended longitudinally across the lesion cores and seemed to be aligned with astrocyte glia. In the control or IgG treated animals, however, very few axons stopped at astrocyte ‘wall’ (Figure 9A). Quantification of NF-200 immunostaining displayed that administration of neutralizing antibodies led to significantly increased numbers of axons at the lesion site compared to those in control or IgG treated animals (Figure 9B). In support, western blot results showed upregulation of NF-200 (Figures 9C and 9D). Furthermore, blocking A1 astrocytes strikingly facilitated 5-HT axon regeneration through the lesion core filled with astrocytic scar barriers, and penetrated into the caudal end (Extended Data Figure 11). This was in drastic contrast to the control groups, in which almost no detectable 5-HT fibers could be observed beyond the lesion site (Extended Data Figure 11). Electrophysiological assay was further conducted to verify restoration of functional connectivity (Figure 9E). Animals treated with neutralizing antibodies exhibited evoked action potential similar to that of the intact animals, with amplitudes remarkably higher than that of control or IgG treated (Figures 9F and 9G), indicating the formation of some kind of new synaptic relays. More

importantly, re-transection of the spinal cord at place rostral to the first lesion completely abolished the recovered action potentials (Figures 9F and 9G). Collectively, these data indicated that blockade of A1 astrocytes promoted axon regeneration across the lesion site or induced the reconstruction of local neural circuitry inside the injury site.

DISCUSSION

Neuronal cell death is the major reason underlying the loss of sensory, motor, and cognitive functions after neural injuries or neurodegenerative events. Replacement of lost neurons can be achieved through transplantation of embryonic stem cells or iPSCs followed by induced neurogenesis [39-42] , in vivo reprogramming for glia-neuron trans-differentiation (Gascón et al., 2016; Guo et al., 2014; Tai *et al.*, 2021), or activation of endogenous NSCs. Stem cell transplanting strategy to date still has several key problems, such as cell survival, efficient neuronal differentiation, and potential tumorigenesis [43]. In vivo reprogramming of glial cells is emerging to be a great approach, but some limitations about precise glial targeting or accurate differentiation into specific neuronal types still remain [44, 45]. Limited number of NSCs still remain in the mature CNS. Although activation and neuronal differentiation of endogenous NSCs has been reported in the brain hippocampus, the NSCs in the adult spinal cord often fail. One likely reason for such failure in the spinal cord is due to the local microenvironment not supporting endogenous NSC activation and

neuronal differentiation.

This study identified UCHL1 as a key positive regulator of spinal cord endogenous NSC activation and neuronal differentiation. Specifically, SCI led to down-regulation of UCHL1 in NSCs downstream of C3 signaling produced by A1 reactive astrocytes. Therefore, direct overexpression of UCHL1 in the NSCs resulted in their activation and neuronal differentiation via UCHL1's function to clear intracellular protein aggregates through ubiquitin-proteasome approach. As a result, overexpression of UCHL1 or blockade of A1 astrocytes led to Nestin^{+} endogenous NSC activation and improved neural circuit repair, which in turn promoted motor functional recovery after SCI. Our findings revealed that the endogenous spinal cord NSCs were negatively controlled by A1 astrocytes mediated inactivation of the UCHL1-proteasome pathway, providing new insights into the non-neurogenic pathological milieu of mature spinal cord after SCI.

The deficiency of neurogenesis in adult spinal cord largely attributes to the failure of endogenous NSC activation and neuronal differentiation. Single-cell RNA sequencing analysis revealed that Nestin^{+} cells outside the central canal are endogenous NSCs being activated upon SCI [37]. Consistently, under control condition an increase of Nestin/SOX2^{+} cells and proliferating Ki-67/Nestin^{+} cells in response to SCI were also observed here near the lesion location, suggesting the activation of endogenous NSCs post-SCI. However, it usually fails to support effective neural regeneration and function recovery

upon this limited mobilization of NSCs under the inhibitory microenvironment.

Insoluble protein aggregations are importantly factors in stem cell activation, proliferation and differentiation. Protein homeostasis of NSCs and progenitor cells are proteolytically processed by UPS, in which several ubiquitin ligases and deubiquitinating enzymes, including UCHL1, play essential roles [23]. Quiescent NSCs can clear protein aggresomes via vimentin-mediated proteasome localization during activation, and Nestin$^+$ NSCs in vimentin KO mice have a decreased ability to exit quiescence status In vivo [15]. Consistently, our study observed that spinal cord Nestin$^+$ NSCs overexpressing UCHL1 possessed an enhanced ability to proliferate and give rise to neurons both in vitro and in vivo. The results were consistent to a previous study that UCHL1 promoted neuronal differentiation and neurogenesis of Nestin$^+$ progenitors in the embryonic brain [46]. The mechanism underlying the neurogenic role of UCHL1 in NSCs has been shown to be due to its regulatory effects on ubiquitin level as previously described [46, 47]. Our study was also in line with the study that removal of protein aggregates by enhancing lysosome activity improved the capacity of quiescent NSCs to be activated [14]. Thus, it is likely that lysosomes and proteasomes act synergistically in protein aggregation clearance to control NSC activation. But it is also noteworthy that proteasome and UCHL1 could also enhance SCI recovery by protecting motoneuron from death and enhancing neural regeneration after spinal cord trauma [23], which could possibly contribute to the

function restoration observed here in some way.

The molecular mechanism underlying impaired proteasome and UCHL1 function in the spinal cord NSCs is mostly unknown. Based on protein microarray analysis of CSF, we found C3 and some other astrocyte markers were remarkably upregulated in SCI animals. Moreover, we demonstrated that A1 astrocytes identified in the lesion site were the source of the increased level of C3 after SCI. A1 astrocytes [28] are neurotoxic and propagate inflammatory during neurodegeneration. Their inappropriate activation, together with the subsequent C1q/C3 complement pathway, are involved in the impaired clearance of cellular debris and the formation of amyloid β (Aβ) plaques in aging or AD related neurons [30, 34, 48, 49]. In consistent, our results showed that C3 led to increased protein aggregates in NSCs, accompanied by impaired proteasome activity and reduced cell proliferation. Furthermore, we found that A1 astrocytes induced by TNFα/IL-1α/C1q significantly suppressed NSC proliferation and neuronal differentiation through C3-mediated inhibition of aggregations clearance. Oxidized proteins often aggregate into toxic protein complex resistant to proteasome-mediated proteolysis after severe injury [24]. Using C3R and ROS inhibitor, we showed that C3/ROS/Nrf2 signaling was likely involved in the inhibition of UCHL1 and UPS activity mediated by A1 astrocytes. Blockade of A1 astrocytes has been shown to preserve neurons and alleviate axonal damage by inhibiting neuroinflammation after optic nerve crush or SCI [28, 31, 32]. Here, we provided novel evidence that abolishment of A1

reactive astrocytes with neutralizing antibodies could facilitate nerve regeneration and partial motor functional recovery by promoting NSC activation and neuronal differentiation through UCHL1-proteasome function. Together, these results suggest that A1 astrocytes activated after SCI might be one of the local environmental factors contributing to the non-neurogenic environment in the adult spinal cord. They then act through C3 signaling to down regulate UCHL1 and impair UPS function in NSCs. Mobilizing endogenous NSCs to enhance intrinsic neural regeneration after SCI is a challenging task of great importance. The present study revealed that A1 astrocytes, C3 signaling, and UCHL1 associated proteasome function might be potential therapeutic targets for spinal cord regeneration after SCI.

The present study mainly focused on the regulatory mechanism underlying the activation the endogenous spinal cord NSCs after SCI. Although it remains debating what cells are considered endogenous NSCs in in the spinal cord, here we identified the endogenous NSCs as Nestin^{+} cells, majority of which were also Sox2^{+}. Future studies can be performed to more specifically target endogenous NSCs for genetic manipulation in the adult spinal cord in vivo.

Methods

Animals

All experimental procedures using laboratory animals were conducted in accordance with the Guide for the Care and Use of Laboratory Animals (National Research Council, 1996) and approved by the Animal Care and Use Committee of Sun Yat-sen University. Female Sprague Dawley (SD) rats (age, 8~10 weeks; weight, 180~200 g) and BALB/C mice (half male and female; age, 8~10 weeks; weight, 20~30 g) were purchased from the Guangdong Medical Laboratory Animal Center and housed under standard specific pathogen free (SPF) condition. All animals were housed in standard cages under a regulated environment (12-h light/dark cycle) with free access to food and water about 1 week before surgery.

NSCs Culture and Differentiation

NSCs were obtained from the fetal brain of embryonic14-day SD rats. Briefly, the cerebrum of embryos was dissected out and the covering pia mater and blood vessels were removed under a microscope. Then the brain was mechanically dissociated in pre-cooling phosphate-buffered saline (PBS) to generate a single cell suspension and centrifuged at 1000 revolutions per minute (rpm) for 10 min. The cell pellet was resuspended and cultured with DMEM/F-12 medium (Gibco, Life Technologies, USA) supplemented with 2%

B-27™ supplement (50X; Gibco, Life Technologies, USA), 20 ng/ml growth factor (EGF; Peprotech, New Jersey, USA), 20 ng/ml fibroblast growth factor (FGF; Peprotech, New Jersey, USA), and 1% penicillin/streptomycin (10,000 U/ml, Gibco, Life Technologies, USA). NSCs were purified by passaged every 3 days, and cells between passages 2~5 were selected to perform further investigation.

For NSCs differentiation, the cells pellets were digested into single cells with Accutase (Millipore, Bedford, MA), and subjected to neuronal differentiation on 0.1% poly-L-lysine (Gibco, USA) coated culture dishes in Neurobasal (Gibco, Life Technologies, USA) supplemented with 2% B-27™. The medium was changed every 2-3 days.

Astrocytes Culture and Induction

Astrocytes were isolated from postnatal 2-day SD rats. After stripping the meninges and blood vessels, cortices were mechanically then enzymatically dissociated into single-cell suspension with 0.25% trypsin at 37℃ for 15 min, followed by filtration and centrifugation to collect cell pellets. Cells were suspended with basal medium (DMEM/F-12; 10% fetal bovine serum, FBS) and plated on uncoated plates for 30 min to remove fibroblasts and endothelial cells. Subsequently, the non-adherent astrocytes were transferred into new dishes pre-coated with 0.1% poly-L-lysine. The cell medium was changed every 3 days and passaged when the cell fusion rate reached approximately

90%. Astrocytes were shaken at 200 r/min overnight to remove upper layer microglia that were attached to the surface of astrocytes to further purify astrocytes before passage. To induce A1 astrocytes, cells were incubated with the triple factors TNFα (30 ng/ml), IL-1α (3 ng/ml) and C1q (400 ng/ml) for 24 h and the successful induction of A1 astrocytes was verified by highly increased $C3^+$ astrocytes formation via immunofluorescent staining and flow cytometry assay.

Lentivirus-mediated Overexpression of UCHL1

The lentivirus overexpressing UCHL1 (OE-UCHL1-LV) and empty lentiviral vector (NC-LV) were constructed by HanBio Technology (Shanghai, China). Lentivirus designed to overexpress UCHL1 were cloned into the pHBLV-CMV-MCS-3FLAG-EF1-GFP-T2A-PURO lentiviral vector containing the ZsGreen reporter gene. The lentivirus vectors were transferred into 293T cells in the presence of packaging plasmids (psPAX2 and pMD2G) using Lipofiter™ (HanBio Technology) for lentivirus packaging. 293T cells were transfected and the overexpression efficacy were assessed after 48 h by qPCR. The final lentiviral vector titer was 2×10^8 TU/ml.

For NSCs infection, cells were transfected with diluted lentiviral solution with a multiplicity of infection (MOI) of 25, with supplement of 1 mg/ml polybrene. At 24 h after transfection, the medium was replaced with fresh basal medium (FBS-free) without penicillin/streptomycin for further 24 h. GFP

expression was visualized under fluorescent microscope at 48 h post-transfection, and over-expression of UCHL1 was determined by Western blot and qPCR analysis.

Co-culture of NSCs and Astrocytes

Two in vitro co-culture systems were conducted here (Figure 4E): Ⅰ. We used a transwell system that allowed interaction via diffusible factors. Unstimulated Control astrocytes or A1 astrocytes in the transwell were on the top of NSCs in the lower chamber, and both cells were cultured within the basal culture medium (free of FBS) of NSCs. Ⅱ. a simple astrocytes conditional medium (ACM) transfer from the Control/A1 astrocytes cultures to NSCs' cultures. After incubation in the normal or A1-inducing medium, astrocytes were cultured with the basal culture medium (free of FBS) of NSCs for another 24h, then the ACM from the Control astrocytes or A1 astrocytes were collected and added into the basal medium of NSCs at a ratio of 1:1 ACM to NSCs culture medium. The cell proliferation, aggresome formation and proteasome activity was assessed at 24 h later.

Cell Proliferation Assay

Cell proliferation in vitro was examined by EdU incorporation. NSCs were incubated with a culture medium supplemented with 10 μM EdU overnight before harvesting. Cells were fixed with 4% paraformaldehyde (PFA) followed

by permeabilization, then washed twice with 3% bovine serum albumin (BSA) and stained using Click-iT EdU assay kit (US Everbright INC.) in accordance to the manufacturer's instructions. After washed once, the cells were resuspended with Hoechst solution (2 ug/ml; US EVERBRIGHT INC.) for DNA counterstaining prior to analysis on Cytoflex LX or laser scanning confocal microscope (LSCM). The control cells that were not subjected to EdU but underwent fluorescent EdU detection were used as a negative base to assess cutoff values for EdU positivity.

Proteostat Analysis

Cells were fixed as mentioned above, then permeabilized with 0.5% Triton X-100/PBS on ice and gently shake for 30 min. After washed twice with PBS, cells were resuspended with PROTEOSTAT Aggresome Detection Reagent (1:2000) and protected from light at room temperature (RT) for 30 min, and subsequently counterstained with Hoechst 33342 (1:1000). The stained cells were analyzed using confocal microscope. For flow cytometry, 500 ul of freshly diluted 1:10000 PROTEOSTAT Aggresome Detection Reagent was applied to incubate cells for 30 min under protection from light. A nutrient deprivation assay that cleared proteostat and a proteasome inhibitor were conducted as controls. MG132, a proteasome inhibitor accelerating the formation of perinuclear aggresome within cells, was used as a positive control. For nutrient deprivation, cells were incubated in HBSS (Gibco) supplemented with 1 mM

HEPES that prevented over-acidification for 3 h, then the medium was replaced with basal culture medium.

Proteasome Activity Assay

Proteasome activity assays were performed by a proteasome activity probe according to the instructions. The treated cells were incubated with the 5 μM proteasome activity probe Me4BodipyFl-Ahx3Leu3VS (Boston Biochem) for 2 h at 37°C, then washed and analyzed via flow cytometry.

Enzyme Linked Immunosorbent Assay (ELISA)

The C3 level in the peripheral blood and CSF collected from SCI rats were detected through RayBio huMan C3a ELISA kit (RayBiotech) following the manufacturer's instructions. Briefly, 100 μl standard or sample was added to each well and incubated 2.5 h at RT with gentle shaking, then washed four times and incubated with biotinylated antibody for 1h. 100 μl HRP-conjugated Streptavidin was subsequently added, followed by incubation of 3,3,5,5'-tetramethylbenzidine (TMB) one-step substrate reagent for 30 min at RT in the dark with gentle shaking. Finally, terminating the action with stop solution and the absorbance value at 450 nm was measured and recorded immediately.

Spinal Cord Injury Model and Postoperative Care

To produce the 10th thoracic vertebra (T10) section SCI model, animals were anesthetized and the back fur was shaved and disinfected with Iodine Volts Swab. An approximately 2 cm incision was made on the T9-T11 skin, then the fat, fascia layer and paravertebral muscles were separated successively to expose the T10 vertebra. Then T10 laminectomy was performed and T10 spinal tissue was transected completely using a sharp scalpel. After hemostasis, rats were randomly divided into six groups, and a total of 10 μl specific transplant was injected into the lesion site using a microsyringe according to the animal groups as follows: Sham group (no SCI; n=12); lesion control group (PBS; n=12); empty lentiviral vector (NC-LV；2×10^8 TU/ml; n=12); lentiviral vector encoding UCHL1 (OE-UCHL1-LV; 2×10^8 TU/ml; n=12) group; recombinant human UCHL1 (rh-UCHL1; 4 μM; n=12) group; and the LDN-57444 (UCHL1 inhibitor; 2 mM; n=12) group. A total of 5 μl grafts was separately mixed with 5 μl Matrigel before transplanted into the lesions of SCI rats to avoid loss.

To block A1 astrocytes after SCI using neutralizing antibodies [28], BALB/C mice were used. Expect for the Sham group (without SCI; n=12), mice were underwent complete T10 transection SCI and injected with triple neutralizing antibodies (Neutralizing Abs group; TNFα/IL-1α/C1q, 10 mg/kg each; n=12), the control IgG antibody (IgG group; 10 mg/kg; n=12) and 0.9% normal saline (Lesion control group; n=12) via intraperitoneal injection once a week, separately.

The body temperature of animals was maintained at about 37°C using a heating pad during the entire surgery until revival fully from anesthesia. During postoperative care, animals underwent manual bladder evacuations till autonomous urination restoration, and checks daily for wounds, infection, weight loss, autophagy of toes and mobility. All animals used in this experiment did not show wound infection, erosion or self-induced wounds.

Tissue Preparation

At the corresponding of experimental endpoints, the animals were perfused with 0.9% normal saline followed by 4% PFA in 0.1 M PBS (pH 7.2), then the spinal cord was dissected, post-fixed for 6~8 hours and dehydrated in 20% and 30% sucrose for 3 days successively. After embedded in Tissue-Tek O.C.T. (Sakura), 14 μm thickness of the cross sections and 1.5 cm longitudinal slices of spinal cords containing the lesion site were collected on a cryostat.

Immunofluorescent Staining

For immunocytochemistry analysis, the cells were fixed with 4% PFA and permeabilized using 0.5% Triton X-100, then blocked in 5% BSA for 1 hour at RT. For immunohistochemistry, the frozen sections of the spinal cord were washed in PBS for 15 mins, subsequently underwent antigen retrieval using Proteinase K and blocking with 5% BSA supplemented with 0.3% Triton X-100 for 2 hours. After the blocking procedure, the fixed cells and slices were

incubated with the first antibodies overnight at 4℃. The first antibodies used in the present study included: UCHL1 (1:300; Cell Signaling Technology, CST), Nestin (1:300; Cell Signaling Technology, CST), SOX2 (1:300; Abcam), Glial Fibrillary Acidic Protein (GFAP; 1:300; Cell Signaling Technology, CST), Microtubule Associated Protein 2 (MAP2; 1:300; Abcam), Neurofilament 200 (NF200; 1:300; Cell Signaling Technology, CST), 5-hydroxytryptamine (5HT; 1:5000), Myelin Basic Protein (MBP; 1:300; Cell Signaling Technology, CST), NeuN (1:300; Abcam), C3 (1:10; Abcam), C3aR (1:200; Santa Cruz), NG2 (1:200; Santa Cruz), Doublecortin (DCX; 1:300; Abcam), Ki-67 (1:300; Abcam), Tubulin β3 (1:300; Cell Signaling Technology, CST). Post washing in PBS for three times, cells and sections were subsequently incubated with Alexa Flour 488/594/647-conjugated secondary antibodies and counterstained with DAPI (1:5000; Sigma). Immunofluorescence staining was examined using a confocal microscope.

Behavior Test

The Basso, Beattie & Bresnahan (BBB) locomotor rating test was performed at 2 days before injury, 1~3 days and weekly post-surgery to evaluate the motor functions of hindlimbs. Rats were placed on a quiet and open plan to ensure spontaneous movement, then the walking and physical activities of hind limbs were observed and recorded. BBB scale comprises three parts: Ⅰ. the joints movement of hind limbs, which scored 0~7; Ⅱ. the gait and coordination

function of the hind limbs, which scored 8~13; Ⅲ. the fineness of the paw in motion, which scored 14~21. Behavior evaluation was conducted weekly post-SCI by two investigators familiar with the BBB criteria but blinded to the experimental groups, separately.

Protein Microarray of Cerebrospinal Fluid from SCI Animals

Cerebrospinal fluid (CSF) was extracted using paracentesis from the cerebellomedullary cistern. Briefly, at 6 h after T10 complete transection SCI, rats (n=4) were re-anesthetized and fixed with a stereotaxic apparatus. Then the occipital protuberance was exposed, and a glass capillary was inserted into the cerebellomedullary cistern carefully through the occipital bone. Approximately 100~120 μl CSF was collected from each rat and kept at -80°C for further investigation. CSF samples from an equal number of rats (n=4) without surgery were used as the control.

Protein microarray analyses of CSF harvested from the normal/SCI rats were performed by G-Series Rat Cytokine Array 67 (RayBiotech, Inc., Guangzhou, China) accordingly to the manufacturers' instructions. A total of 100 μl sample from each rat was used and raw data obtained was conducted background subtraction and normalization before clustering analysis. Gene ontology (GO) annotation, consisting of three parts including molecular function, biological process and cellular component, was applied to identify functions of potential genes. Possible signaling pathways involved in were

analyzed by the Kyoto Encyclopedia of Genes and Genomes (KEGG) database.

Electrophysiology Examination

Electrophysiological evaluation was carried out as previously described [10, 50] at 8 weeks after SCI in rats or 6 weeks post-injury in mice. Animals were re-anesthetized and laminectomy was performed to expose the T7 and T13 spinal cord, which are both 3 segments rostral and caudal to the lesion site. A bipolar stimulating electrode spacing 2 mm was positioned intraspinally at the rostral T7 segment, and a silver ball electrode placed at the caudal T13 segment to record evoked response. 0.1 ms square wave pulse was delivered at 10 ms interval and field activity was amplified and recorded. At least 20 trails from each recording site were averaged and the amplitude of evoked potential was quantified.

Quantitative Real-time Polymerase Chain Reaction (qPCR)

Total RNA from NSCs or spinal cord tissues was extracted using Trizol (Invitrogen, life technologies) according to the reagent specification. The quantality of RNA yield was determined by the Nanodrop one (ThermoFisher). Total RNA was subjected to reverse transcription into cDNA using the PrimeScript RT reagent Kit (Vazyme). qPCR assay was conducted using the SYBR Premix EX Taq (Vazyme). The expression levels were normalized to

those of glyceraldehyde 3-phosphate dehydrogenase (GAPDH). Relative expression of genes was calculated as fold changes using the $2^{-\triangle\triangle Ct}$ method. The primer sequences for genes were provided in Table 1.

Western Blotting

Western blot was conducted to detect the protein enrichment in cells and spinal tissues. In brief, cells and spinal cord containing the lesion site were lysed in PIPA (Solarbio) supplemented with PMSF (1:100; Solarbio) and ultrasonic splitting on ice. Total of 20 μg protein was run on 10%-12% sodium dodecyl sulfate-polyacrylamide electrophoresis (SDS-PAGE) gel, transferred to polyvinylidene difluoride (PVDF; Millipore, Mississauga, Canada) membranes and blocked with 5% no-fat milk. Then membranes were incubated with first antibodies overnight at 4°C with gentle shaking, followed by combined with horseradish peroxidase (HRP)-conjugated secondary antibodies (1:1,000). Protein enrichment was visualized via chemiluminescence reagent and the grayscale analysis of bands was determined using Image J. First antibodies applied in this study are as follows: UCHL1 (1:1000; Cell Signaling Technology, CST), Nestin (1:1000; Cell Signaling Technology, CST), GFAP (1:1000; Cell Signaling Technology, CST), MAP2 (1:1000; Abcam), NF200 (1:1000; Cell Signaling Technology, CST), MBP (1:1000; Cell Signaling Technology, CST), nuclear related factor 2 (Nrf2; 1:1000; Abcam), C3 (1:1000; Abcam), C3aR (1:500; Santa Cruz), GAPDH

(1:1000, Beyotime Biotechnology), β-actin (1:1000, Beyotime Biotechnology). GAPDH and β-actin were used as the internal controls.

Quantification and Statistical Analysis

SPSS (Version 20.0; Abbott Laboratories, Chicago, IL) was applied for statistical analysis. Independent, Two-tailed unpaired Student's t-test was used for comparisons between two groups. For multiple comparisons, One-way Analysis of variance (ANOVA) followed by Tukey HSD post-hoc analysis or Kruskal Wallis test with Bonferroni correction analysis was selected. And Two-way ANOVA with Tukey HSD was conducted for BBB scores analysis. All data was presented as mean ± the standard error of the mean (SEM) and $p < 0.05$ was deemed statistically significant.

Acknowledgements

We thank Krsna Muscheck for helpful suggestions and revision on the manuscript. This study was supported by the National Natural Science Foundation of China (NSFC; 82071362) and Basic Research Project of Shenzhen Science and Technology Innovation Commission (JCYJ20190809165201646).

Author contributions

L.D. and D.Y.B.D. designed the experiments. L.D., W.W.C. performed the

experiments and analyzed the data. X.Y., and M.S. helped with the behavior tests and histology experiments. L.D. wrote the manuscript. W.W.C., M.S., T.L., L.L., F.-Q.Z. and D.Y.B.D. revised the paper. All authors reviewed and approved the manuscript.

Competing interests

The authors declare no competing interests.

REFERENCES

1. Assinck, P., Duncan, G.J., Hilton, B.J., Plemel, J.R. & Tetzlaff, W. Cell transplantation therapy for spinal cord injury. *Nat Neurosci* **20**, 637-647 (2017).

2. Guo X, F.Y., Sun T, Feng S, Tang J, Chen L, Cao X, Lin H, He X, Li M, Zhang Z, Yin G, Mei X, Huang H. Clinical guidelines for neurorestorative therapies in spinal cord injury. *J Neurorestoratology* **9**, 31-49 (2021).

3. Zhuang M, W.Q., Wan F, Hu Y. State-of-the-art non-invasive brain–computer interface for neural rehabilitation: A review. *J Neurorestoratology* **8**, 12-25 (2020).

4. Stenudd, M., Sabelström, H. & Frisén, J. Role of Endogenous Neural Stem Cells in Spinal Cord Injury and Repair. *JAMA Neurology* **72**, 235 (2015).

5. Barnabé-Heider, F. & Frisén, J. Stem Cells for Spinal Cord Repair. *Cell Stem Cell* **3**, 16-24 (2008).

6. McTigue, D.M. & Sahinkaya, F.R. The fate of proliferating cells in the injured adult spinal cord. *Stem Cell Research & Therapy* **2**, 7 (2011).

7. Liu, Y.*, et al.* Endogenous neural stem cells in central canal of adult rats acquired

limited ability to differentiate into neurons following mild spinal cord injury. *Int J Clin Exp Pathol* **8**, 3835-3842 (2015).

8. Barnabé-Heider, F.*, et al.* Origin of New Glial Cells in Intact and Injured Adult Spinal Cord. *Cell stem cell* **7**, 470-482 (2010).

9. Tai, W.*, et al.* In vivo reprogramming of NG2 glia enables adult neurogenesis and functional recovery following spinal cord injury. *Cell stem cell* (2021).

10. Lu, P.*, et al.* Long-Distance Growth and Connectivity of Neural Stem Cells after Severe Spinal Cord Injury. *Cell* **150**, 1264-1273 (2012).

11. Rao, J.-S.*, et al.* NT3-chitosan enables de novo regeneration and functional recovery in monkeys after spinal cord injury. *Proceedings of the National Academy of Sciences* **115**, E5595-E5604 (2018).

12. Rouanet, C., Reges, D., Rocha, E., Gagliardi, V. & Silva, G.S. Traumatic spinal cord injury: current concepts and treatment update. *Arquivos de neuro-psiquiatria* **75**, 387-393 (2017).

13. Vilchez, D., Simic, M.S. & Dillin, A. Proteostasis and aging of stem cells. *Trends in cell biology* **24**, 161-170 (2014).

14. Leeman, D.S.*, et al.* Lysosome activation clears aggregates and enhances quiescent neural stem cell activation during aging. *Science (New York, N.Y.)* **359**, 1277-1283 (2018).

15. Morrow, C.S.*, et al.* Vimentin Coordinates Protein Turnover at the Aggresome during Neural Stem Cell Quiescence Exit. *Cell Stem Cell* **26**, 558-568 e559 (2020).

16. Liu, H.*, et al.* The point mutation UCH-L1 C152A protects primary neurons against cyclopentenone prostaglandin-induced cytotoxicity: implications for post-ischemic neuronal injury. *Cell death & disease* **6**, e1966 (2015).

17. Liu, Y., Fallon, L., Lashuel, H.A., Liu, Z. & Lansbury, P.T., Jr. The UCH-L1 gene encodes two opposing enzymatic activities that affect alpha-synuclein degradation and Parkinson's disease susceptibility. *Cell* **111**, 209-218 (2002).

18. Gong, B.*, et al.* Ubiquitin hydrolase Uch-L1 rescues beta-amyloid-induced decreases in synaptic function and contextual memory. *Cell* **126**, 775-788 (2006).

19. Bilguvar, K.*, et al.* Recessive loss of function of the neuronal ubiquitin hydrolase UCHL1 leads to early-onset progressive neurodegeneration. *Proceedings of the National Academy of Sciences* **110**, 3489-3494 (2013).

20. Yu, Q.*, et al.* UCH-L1 Inhibition Suppresses tau Aggresome Formation during Proteasomal Impairment. *Mol Neurobiol* **55**, 3812-3821 (2018).

21. Liu, H.*, et al.* Role of UCHL1 in axonal injury and functional recovery after cerebral ischemia. *Proceedings of the National Academy of Sciences* **116**, 4643-4650 (2019).

22. Noor, N.M.*, et al.* Expression and cellular distribution of ubiquitin in response to injury in the developing spinal cord of Monodelphis domestica. *PLoS One* **8**, e62120 (2013).

23. Gong, B., Radulovic, M., Figueiredo-Pereira, M.E. & Cardozo, C. The Ubiquitin-Proteasome System: Potential Therapeutic Targets for Alzheimer’s Disease and Spinal Cord Injury. *Frontiers in Molecular Neuroscience* **9** (2016).

24. Oliva, J. Proteasome and Organs Ischemia-Reperfusion Injury. *International Journal of Molecular Sciences* **19**, 106 (2017).

25. Freeman, M.R. Specification and morphogenesis of astrocytes. *Science (New York, N.Y.)* **330**, 774-778 (2010).

26. Karimi-Abdolrezaee, S. & Billakanti, R. Reactive astrogliosis after spinal cord injury-beneficial and detrimental effects. *Molecular neurobiology* **46**, 251-264 (2012).

27. Escartin, C., *et al.* Reactive astrocyte nomenclature, definitions, and future directions. *Nat Neurosci* **24**, 312-325 (2021).

28. Liddelow, S.A., *et al.* Neurotoxic reactive astrocytes are induced by activated microglia. *Nature* **541**, 481-487 (2017).

29. Hasel, P., Rose, I.V.L., Sadick, J.S., Kim, R.D. & Liddelow, S.A. Neuroinflammatory astrocyte subtypes in the mouse brain. *Nat Neurosci* (2021).

30. Yun, S.P., *et al.* Block of A1 astrocyte conversion by microglia is neuroprotective in models of Parkinson's disease. *Nature Medicine* **24**, 931-938 (2018).

31. Qian, D., *et al.* Blocking Notch signal pathway suppresses the activation of neurotoxic A1 astrocytes after spinal cord injury. *Cell Cycle* **18**, 3010-3029 (2019).

32. Vismara, I., *et al.* Selective Modulation of A1 Astrocytes by Drug-Loaded Nano-Structured Gel in Spinal Cord Injury. *ACS Nano* **14**, 360-371 (2019).

33. Wu, T., *et al.* Complement C3 Is Activated in Human AD Brain and Is Required for Neurodegeneration in Mouse Models of Amyloidosis and Tauopathy. *Cell Reports* **28**, 2111-2123.e2116 (2019).

34. Hong, S., *et al.* Complement and microglia mediate early synapse loss in Alzheimer mouse models. *Science (New York, N.Y.)* **352**, 712-716 (2016).

35. Hu, Z., Tao, L., Liu, Z., Jiang, Y. & Deng, X. Identification of Neural Stem Cells from Postnatal Mouse Auditory Cortex In Vitro. *Stem cells and development* **28**, 860-870 (2019).

36. Kim, K., Higashi, M., Fumino, S. & Tajiri, T. Derivation of neural stem cells from human teratomas. *Stem cell research* **41**, 101633 (2019).

37. Shu, M., *et al.* Single-cell RNA sequencing reveals Nestin(+) active neural stem cells outside the central canal after spinal cord injury. *Sci China Life Sci* (2021).

38. Pickering, A.M., Linder, R.A., Zhang, H., Forman, H.J. & Davies, K.J.A. Nrf2-dependent Induction of Proteasome and Pa28αβ Regulator Are Required for Adaptation to Oxidative Stress. *Journal of Biological Chemistry* **287**, 10021-10031 (2012).

39. Nori, S.*, et al.* Grafted human-induced pluripotent stem-cell-derived neurospheres promote motor functional recovery after spinal cord injury in mice. *Proc Natl Acad Sci U S A* **108**, 16825-16830 (2011).

40. Salewski, R.P.*, et al.* Transplantation of Induced Pluripotent Stem Cell-Derived Neural Stem Cells Mediate Functional Recovery Following Thoracic Spinal Cord Injury Through Remyelination of Axons. *Stem Cells Transl Med* **4**, 743-754 (2015).

41. Harper, J.M.*, et al.* Axonal growth of embryonic stem cell-derived motoneurons in vitro and in motoneuron-injured adult rats. *PNAS* **101**, .7123–7128 (2004).

42. Salewski, R.P., Mitchell, R.A., Shen, C. & Fehlings, M.G. Transplantation of neural stem cells clonally derived from embryonic stem cells promotes recovery after murine spinal cord injury. *Stem Cells Dev* **24**, 36-50 (2015).

43. Vismara, I., Papa, S., Rossi, F., Forloni, G. & Veglianese, P. Current Options for Cell Therapy in Spinal Cord Injury. *Trends in Molecular Medicine* **23**, 831-849 (2017).

44. Li, H. & Chen, G. In Vivo Reprogramming for CNS Repair: Regenerating Neurons from Endogenous Glial Cells. *Neuron* **91**, 728-738 (2016).

45. Qian, C., Dong, B., Wang, X.Y. & Zhou, F.A.-O. In vivo glial trans-differentiation for neuronal replacement and functional recovery in central nervous system. LID - 10.1111/febs.15681 [doi]. (2020).

46. Sakurai, M.*, et al.* Ubiquitin C-terminal hydrolase L1 regulates the morphology of neural progenitor cells and modulates their differentiation. *Journal of cell science* **119**, 162-171 (2006).

47. Naujokat, C. Role of ubiquitin ligases in neural stem and progenitor cells. *Archivum Immunologiae et Therapiae Experimentalis* **57**, 177-188 (2009).

48. Alawieh, A., Elvington, A. & Tomlinson, S. Complement in the Homeostatic and Ischemic Brain. *Frontiers in Immunology* **6** (2015).

49. Rogers, J., Strohmeyer, R., Kovelowski, C.J. & Li, R. Microglia and inflammatory mechanisms in the clearance of amyloid beta peptide. *Glia* **40**, 260-269 (2002).

50. Anderson, M.A.*, et al.* Required growth facilitators propel axon regeneration across complete spinal cord injury. *Nature* **561**, 396-400 (2018).

Figures legends

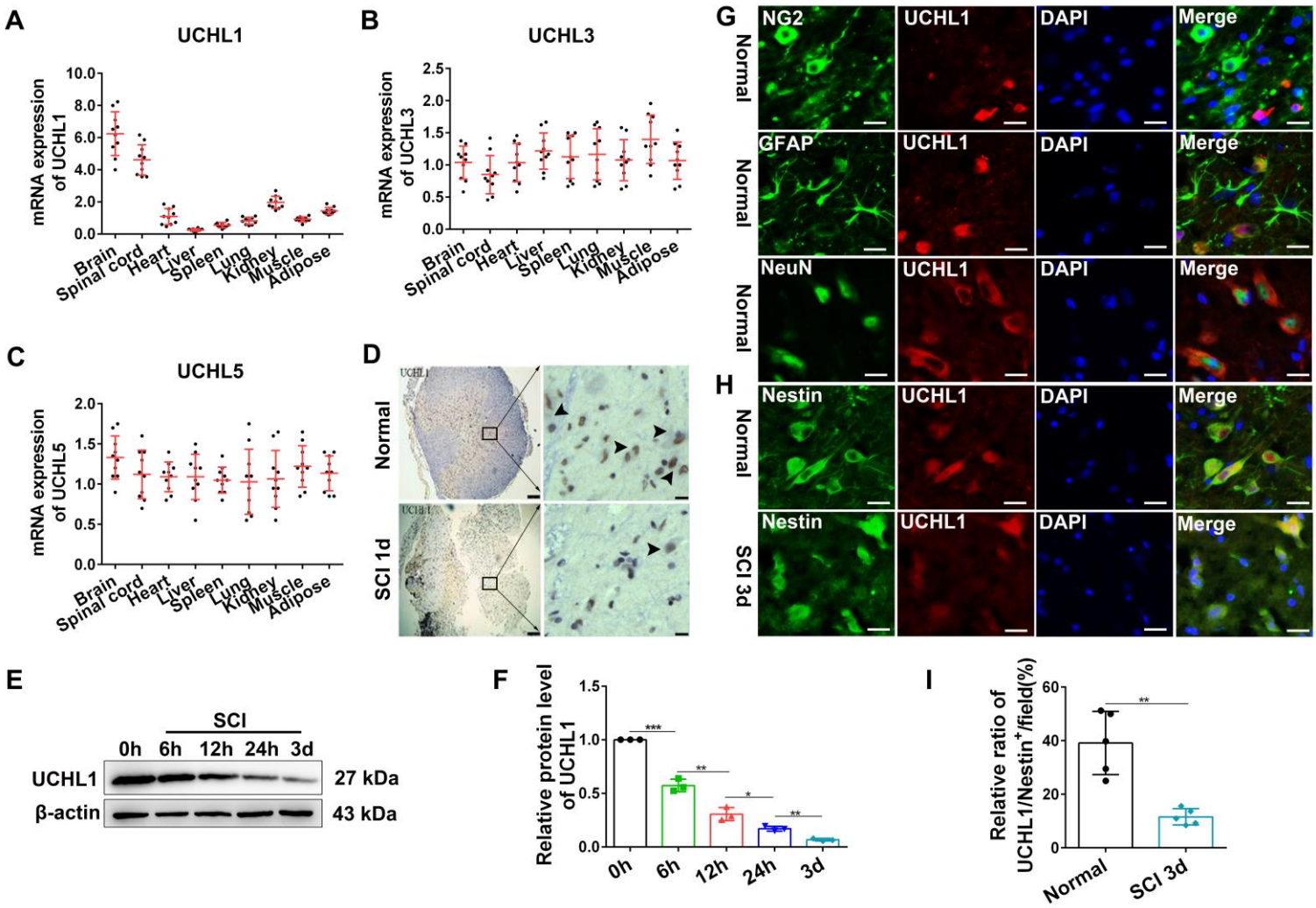

Figure 1 UCHL1 was expressed in the spinal Nestin⁺ NSCs and downregulated remarkably after SCI

(A-C) QPCR analysis showing the relative expression of UCHL1, UCHL3 and UCHL5 in the different organs of rats. UCHL1 was abundantly expressed in the brain and spinal tissues of rats. n=10 independent animals.

(D) Immunohistochemical representative images showed that UCHL1 was remarkably downregulated in the gray matter at 24 h after SCI. Scale bar (left),

100μm, Scale bar (right), 50μm.

(E-F) Western blot analysis was conducted to detect the protein level of UCHL1 in the spinal cord during 3 days post-SCI. Representative immunoblot images and quantification of Western blot assay was shown in E and F. (F) n=3 biological replicates. Data are presented as mean ± SEM. Two-tailed unpaired Student's t-test, 0h vs 6h ***p=0.0002, 6h vs 12h **p=0.0055, 12h vs 24h *p=0.0234, 24h vs 3d **p=0.0021.

(G-H) Immunofluorescence assay shows that UCHL1 was expressed within $NeuN^+$ neurons and $Nestin^+$ NSCs, but not $NG2^+$ Oligodendrogenic progenitor cells and $GFAP^+$ astrocytes according to fluorescent assay. Scale bar, 25μm.

(I) The relative ratio of UCHL1/$Nestin^+$ cells before and at 3 days after SCI. n=5 biological replicates. Data are presented as mean ± SEM. Two-tailed unpaired Student's t-test, **p=0.005.

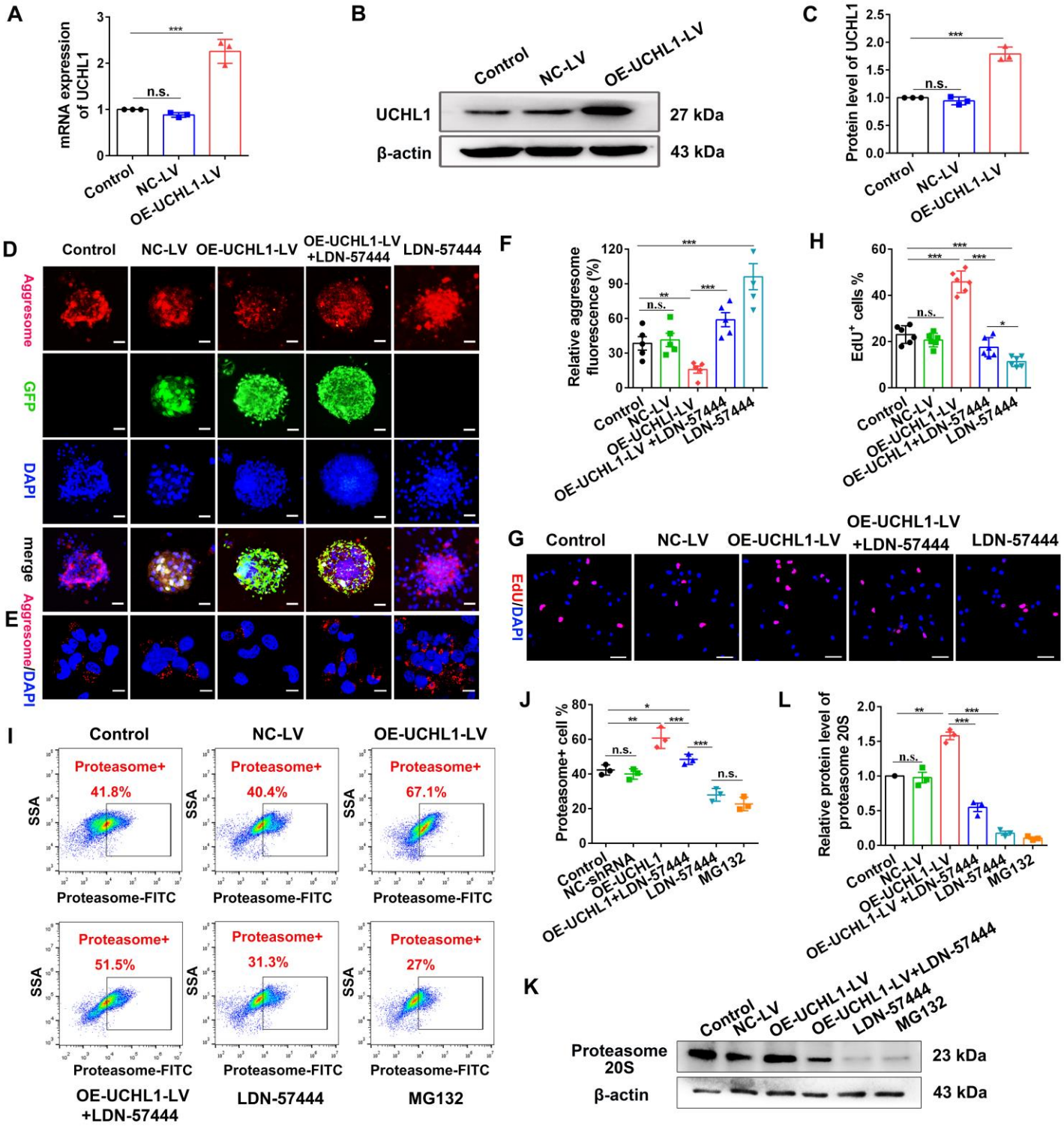

Figure 2 Overexpression of UCHL1 promoted NSCs proliferation by accelerating clearance of protein aggregates via ubiquitin-proteasome pathway in vitro

(A) QPCR analysis showing the mRNA level of UCHL1 in NSCs that were

transfected with either empty lentiviral vector (NC-LV), lentiviral vector encoding UCHL1 (OE-UCHL1-LV) for 48h. n=3 biological replicates. Data are presented as mean ± SEM. Two-tailed unpaired Student's t-test, *p=0.014.

(B-C) Western blot analysis of NSCs transfected with NC-LV or OE-UCHL1-LV for 48h to examine the protein expression of UCHL1. Representative images and quantification of Western blot analysis were shown in B and C. (C) n=3 biological replicates. Data are presented as mean ± SEM. Two-tailed unpaired Student's t-test, **p=0.008.

(D-E) Confocal representative images showing the enrichment of protein aggregates (aggresome^{+}) in NSCs transfected with GFP-NC-LV, GFP-OE-UCHL1-LV, GFP-OE-UCHL1-LV+LDN-57444, or treated with LDN-57444. Scale bar (D), 100μm, Scale bar (E), 100μm.

(F) Quantification of protein aggregates (aggresome^{+}) in NSCs transfected with NC-LV or OE-UCHL1-LV. n=5. Data are presented as mean ± SEM. Kruskal Wallis test with Bonferroni correction, Control vs OE-UCHL1-LV **p=0.0035, OE-UCHL1-LV vs OE-UCHL1-LV+LDN-57444 *p=0.026, OE-UCHL1-LV vs LDN-57444 ***p<0.0001.

(G-H) Confocal representative images and quantification of the proliferating NSCs (EdU/Nestin^{+}) in different treatments. Scale bar (G), 10μm. (H) n=6. Data are presented as mean ± SEM. One-way ANOVA with Tukey HSD post hoc test, Control vs OE-UCHL1-LV ***p<0.0001, OE-UCHL1-LV vs OE-UCHL1-LV+LDN-57444 ***p<0.0001, OE-UCHL1-LV vs LDN-57444

***p<0.0001, OE-UCHL1-LV+LDN-57444 vs LDN-57444 *p=0.041.

(I) The proteasome activity of NSCs in groups was measured by flow cytometry assay. n=3 biological replicates.

(J) Quantification of proteasome activity in NSCs by flow cytometry assay. n=3 biological replicates. Data are presented as mean ± SEM. One-way ANOVA with Tukey HSD post hoc test, Control vs OE-UCHL1-LV **p=0.002, Control vs OE-UCHL1-LV+LDN-57444 *p=0.01, OE-UCHL1-LV vs OE-UCHL1-LV+LDN-57444 ***p=0.000013, OE-UCHL1-LV+LDN-57444 vs LDN-57444 ***p<0.0001.

(K-L) Western blot analysis was performed to detected the protein level of 20S proteasome in NSCs. Representative immunoblot images and quantification of relative protein level were shown in K and L. (L) n=3 biological replicates. Data are presented as mean ± SEM. One-way ANOVA with Tukey HSD post hoc test, Control vs OE-UCHL1-LV ***p=0.000002, OE-UCHL1-LV vs OE-UCHL1-LV+LDN-57444 ***p<0.0001, OE-UCHL1-LV vs LDN-57444 ***p<0.0001, OE-UCHL1-LV+LDN-57444 vs LDN-57444 **p=0.001363.

See also Extended Data Figure 1, Figure 2 and Figure 3.

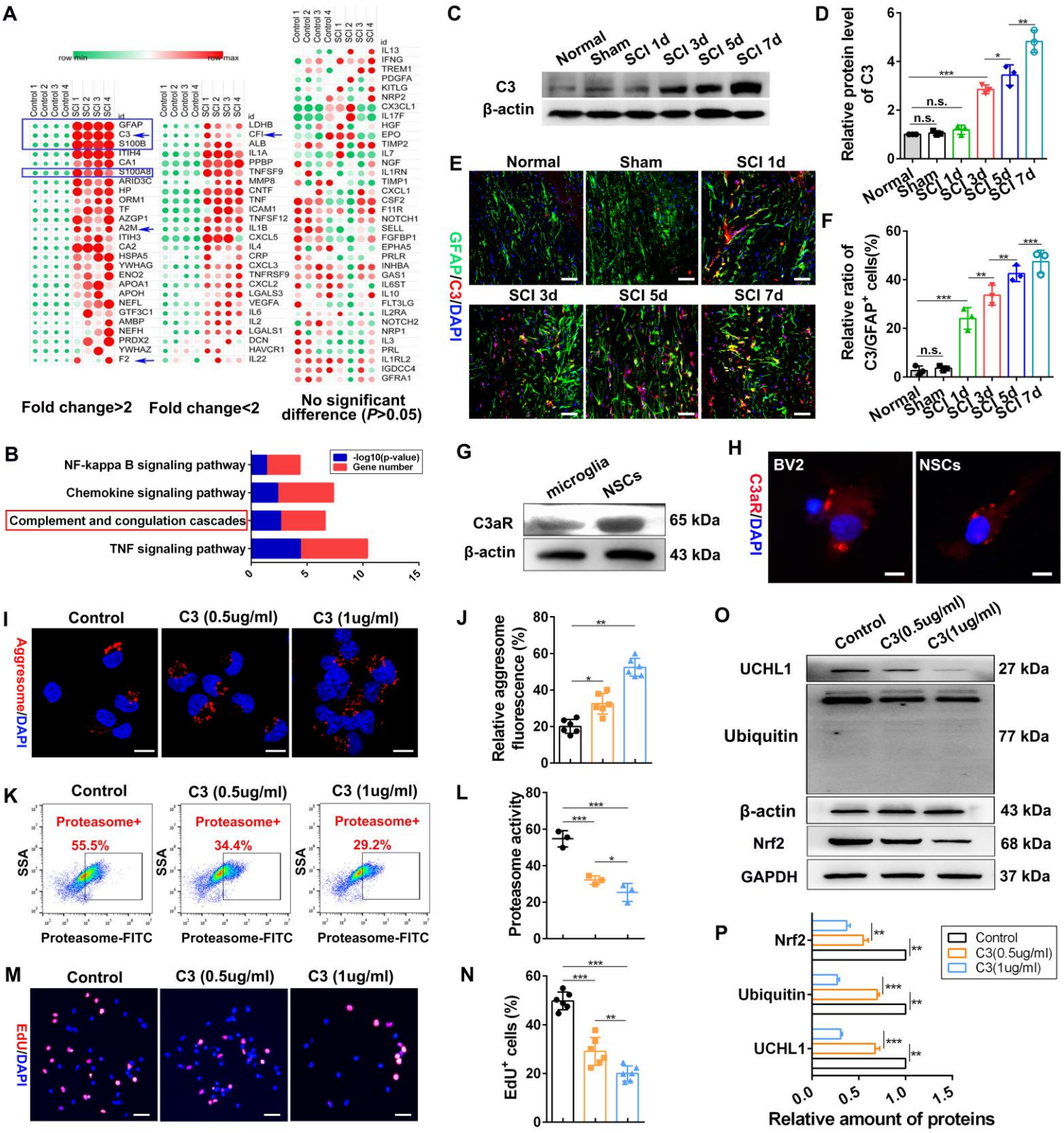

Figure 3 C3 inhibited UCHL1 and induced accumulation of intracellular protein aggregation via C3/Nrf2 pathway to impede NSCs activation

(A) Protein microarray of CSF from intact and SCI rats. CSF was extracted from the intact and SCI rats at 6h post-injury and then conducted for protein microarray analysis with Rat Cytokine Array 67. Scanned array image shows the relative expression changes of cytokines in CSF of SCI rats compared to that of the intact animals. The significantly changed cytokines was screened depending on conditions that the log10(fold change) ＞ log10(1.2) and normalized p value <0.05. n=4 independent animals.

(B) KEGG pathway analysis of differentially expressed cytokines in CSF from intact and SCI rats. The blue bar indicates the -log transformed p value (p<0.05 is considered statistically significant), and the red bar shows the numbers of changed factors in each pathway.

(C-D) Western blot analysis and quantification of the protein level of C3 in the spinal tissues within 7 days post-SCI. (D) n=3 independent animals. One-way ANOVA with Tukey HSD post hoc test, Normal vs SCI 3d ***p=0.000032, SCI 3d vs SCI 5d *p=0.023, SCI 5d vs SCI 7d **p=0.001.

(E) Confocal representative images showing the activation of C3 and $GFAP^+$ astrocytes in spinal tissues within 7 days post-SCI. Scale bar, 25 μm.

(F) Quantification of C3/$GFAP^+$ cells in spinal tissues from Figure 3E. n=3 independent animals. One-way ANOVA with Tukey HSD post hoc test, Normal vs SCI 1d ***p=0.000083, Normal vs SCI 3d ***p=0.000002, SCI 1d vs SCI 3d **p=0.006, SCI 3d vs SCI 5d **p=0.009, SCI 5d vs SCI 7d ***p<0.0001.

(G-H) Western blot analysis and immunofluorescence assay show the

expression of C3aR in BV2 and NSCs. Scale bar (H), 10μm.

(I-J) Immunofluorescence staining (I) and quantification (J) of protein aggregates (aggresome^{+}) in NSCs treated with C3 for 24h. n=3 biological replicates. Scale bar (C), 10μm. (J) n=6 biological replicates. One-way ANOVA with Tukey HSD post hoc test, Control vs C3 (0.5 ug/ml) *p=0.022, Control vs C3 (1 ug/ml) **p=0.005.

(K) Flow cytometry assay revealed the proteasome activity in NSCs treated with C3 for 24h.

(L) Quantification of proteasome activity by flow cytometry assay in treatments. n=3 biological replicates. One-way ANOVA with Tukey HSD post hoc test, Control vs C3 (0.5 ug/ml) ***p=0.000036, Control vs C3 (1 ug/ml) ***p=0.000015, C3 (0.5 ug/ml) vs C3 (1 ug/ml) *p=0.02.

(M) Fluorescent staining with EdU^{+} showed the proliferation of NSCs after cultured with C3 for 24h. Scale bar (E), 25μm.

(N) The percentage of EdU^{+} NSCs was quantified in different groups. n=6 biological replicates. One-way ANOVA with Tukey HSD post hoc test, Control vs C3 (0.5 ug/ml) ***p=0.000002, Control vs C3 (1 ug/ml) ***p<0.000001, C3 (0.5 ug/ml) vs C3 (1 ug/ml) **p=0.007.

(O-P) Expression of UCHL1, Ubiquitin and Nrf2 in NSCs incubated with C3 for 24h was measured by Western blotting. Representative images and quantification of proteins were shown in O and P. (P) n=3 biological replicates. Data are presented as mean ± SEM. One-way ANOVA with Tukey HSD post

hoc test, UCHL1, Control vs C3 (0.5 ug/ml) ***p=0.00066, C3 (0.5 ug/ml) vs C3 (1 ug/ml) ***p=0.000324; Ubiquitin, Control vs C3 (0.5 ug/ml) ***p=0.000053, C3 (0.5 ug/ml) vs C3 (1 ug/ml) ***p=0.000007; Nrf2, Control vs C3 (0.5 ug/ml) ***p=0.000363, C3 (0.5 ug/ml) vs C3 (1 ug/ml) *p=0.036.

See also Extended Data Figure 4.

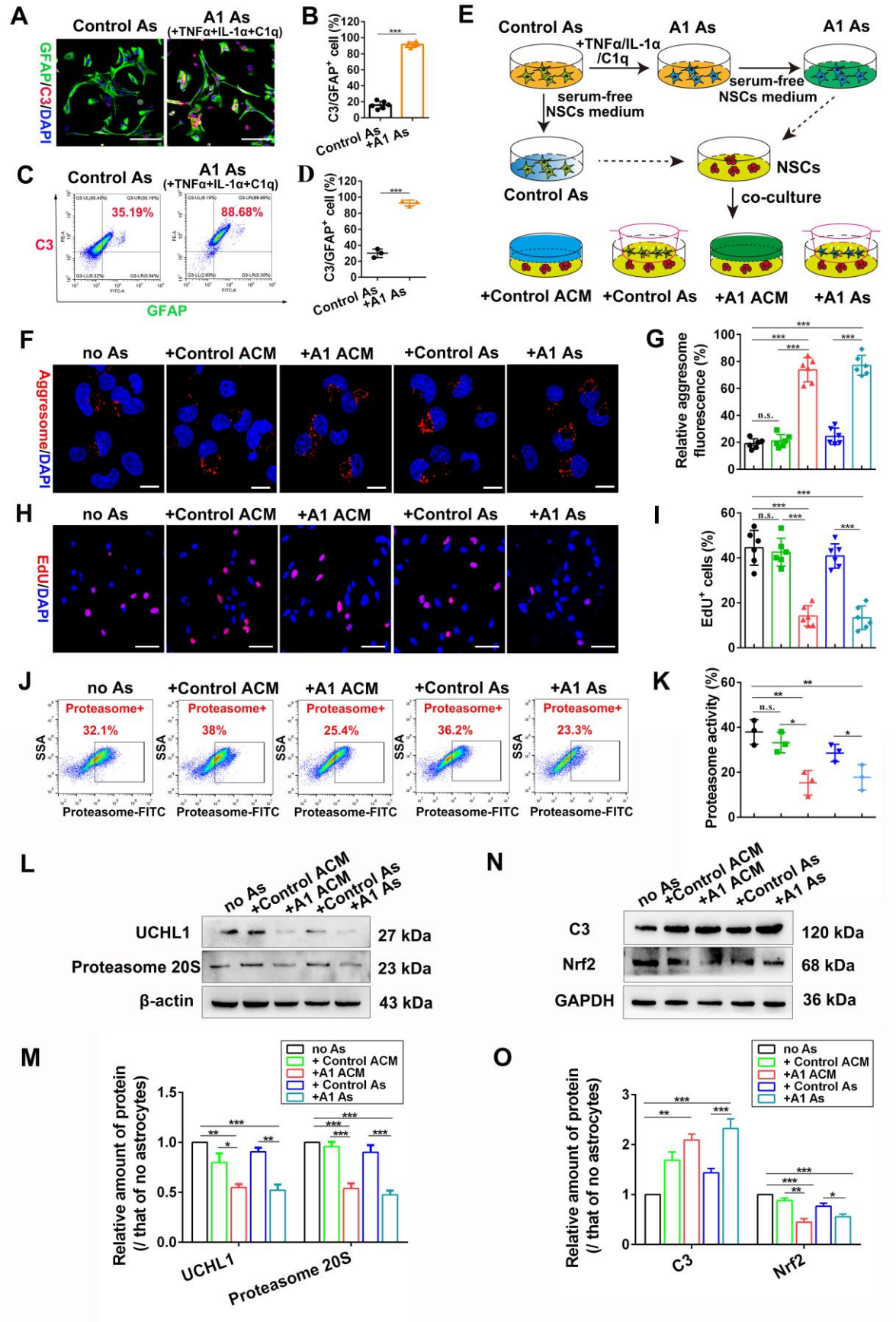

1171 **Figure 4 A1 reactive astrocytes significantly suppressed NSCs activation**

by inducing C3 to inhibit protein aggresome elimination

(A-B) Immunofluorescent staining showing the successful induction of A1 astrocytes, which was confirmed by the highly expressed $C3^+$ astrocytes. Representative images (A) and quantification (B) of $C3^+$ astrocytes were revealed. Scale bar (A), 20μm. (B) n=6 biological replicates. Data are presented as mean ± SEM. Two-tailed unpaired Student's t-test, 0h vs 6h ***p<0.000001.

(C-D) Flow cytometry analysis (C) and quantification (D) of $C3/GFAP^+$ astrocytes induced by TNFα/IL-1α/C1q factors. (D) n=3 biological replicates. Data are presented as mean ± SEM. Two-tailed unpaired Student's t-test, 0h vs 6h ***p=0.000071.

(E) Schematic diagram of the co-culture system of NSCs and astrocytes.

(F-G) Confocal representative images (F) and quantification (G) of protein aggregations identified by aggresome dye in NSCs. Scale bar (F), 10μm. (G) n=6 biological replicates. Data are presented as mean ± SEM. One-way ANOVA with Tukey HSD hoc test, no As vs +A1 ACM ***p<0.000001, no As vs +A1 As ***p<0.000001, +Control ACM vs +A1 ACM ***p<0.000001, +Control AS vs +A1 As ***p<0.000001.

(H) The activation of NSCs was assessed using EdU^+ incorporation assay. Scale bar (H), 25μm.

(I) The histogram shows the quantification of EdU^+ NSCs in the co-culture system. n=6 biological replicates. Data are presented as mean ± SEM.

One-way ANOVA with Tukey HSD post hoc test, no As vs +A1 ACM ***p<0.000001, no As vs +A1 As ***p<0.000001, +Control ACM vs +A1 ACM ***p<0.000001, +Control AS vs +A1 As ***p<0.000001.

(J) Flow cytometry assay revealed the proteasome activity in NSCs co-cultured with astrocytes for 24h.

(K) Quantification of proteasome activity in NSCs co-cultured with astrocytes for 24h. n=3 biological replicates. Data are presented as mean ± SEM. One-way ANOVA with Tukey HSD post hoc test, no As vs +A1 ACM **p=0.002, no As vs +A1 As **p=0.004, +Control ACM vs +A1 ACM *p=0.01, +Control AS vs +A1 As *p=0.025.

(L-M) Western blotting analysis of NSCs after co-cultured with astrocytes or ACM. Representative immunoblots and quantification of UCHL1 and 20S proteasome was revealed in L and M. (M) n=3 biological replicates. Data are presented as mean ± SEM. One-way ANOVA with Tukey HSD post hoc test, UCHL1, no As vs +A1 ACM **p=0.001017, no As vs +A1 As ***p=0.000629, +Control ACM vs +A1 ACM *p=0.049, +Control As vs +A1 As **p=0.003; Proteasome 20S, no As vs +A1 ACM ***p=0.00032, no As vs +A1 As ***p=0.000109, +Control ACM vs +A1 ACM ***p=0.000704, +Control As vs +A1 As ***p=0.000621.

(N-O) Western blotting analysis (N) and quantification (O) of protein level of C3a and UCHL1 in NSCs after co-cultured with astrocytes or ACM. (O) n=3 biological replicates. Data are presented as mean ± SEM. One-way ANOVA

with Tukey HSD post hoc test. C3, no As vs +A1 ACM **p=0.001127, no As vs +A1 As ***p=0.000246, +Control AS vs +A1 As ***p=0.005; Nrf2, no As vs +A1 ACM ***p=0.000165, no As vs +A1 As ***p=0.000979, +Control ACM vs +A1 ACM **p=0.001204, +Control As vs +A1 As *p=0.018.

See also Extended Data Figure 5 and Figure 6.

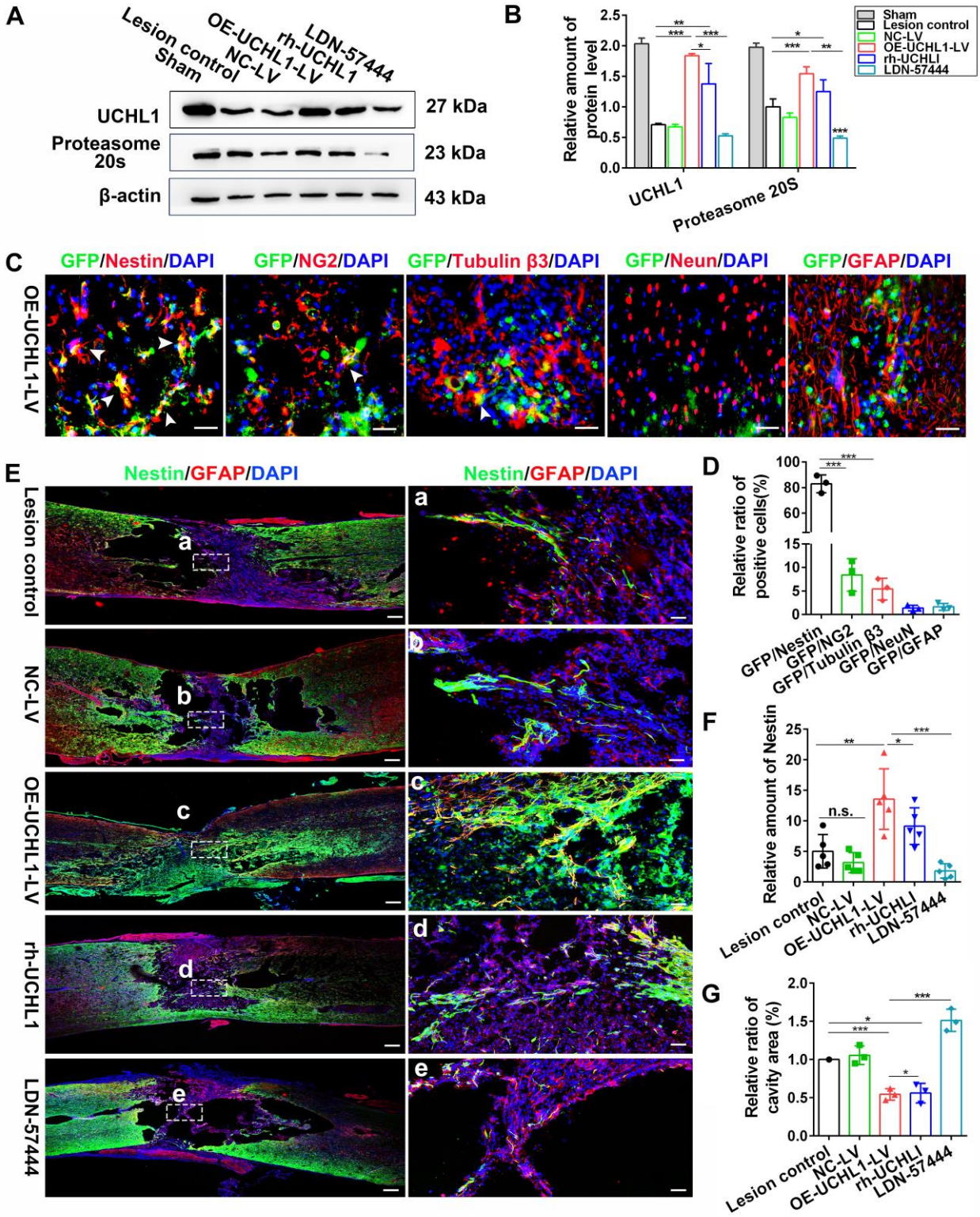

Figure 5 Up-regulation of UCHL1 facilitated activation and migration of endogenous NSCs in lesion site after acute SCI in rats

(A) Western blot analysis of spinal tissues lysate from SCI rats at 7 days after

injury with indicated antibodies.

(B) Quantification of relative expression of UCHL1 and ubiquitin in spinal tissues at 7 days post-SCI**.** n=3 independent animals. n=3 biological replicates. Data are presented as mean ± SEM. One-way ANOVA with Tukey HSD post hoc test, UCHL1, Lesion control vs OE-UCHL1-LV ***p=0.000007, Lesion control vs rh-UCHL1 **p=0.001, OE-UCHL1-LV vs rh-UCHL1 *p=0.02, OE-UCHL1-LV vs LDN-57444 ***p=0.000001; Proteasome 20S, Lesion control vs OE-UCHL1-LV ***p=0.000796, Lesion control vs rh-UCHL1 *p=0.019, OE-UCHL1-LV vs LDN-57444 ***p=0.000001, Lesion control vs LDN-57444 **p=0.001.

(C) Confocal images showing different cells transfected with GFP-OE-UCHL1-LV in vivo at 7-day post-SCI. Scale bar, 20μm.

(D) Quantification of GFP^+ cells in vivo at 7-day post-SCI. n=3 independent animals. n=3 biological replicates. Data are presented as mean ± SEM. One-way ANOVA with Tukey HSD post hoc test, GFP/Nestin+ vs GFP/NG2+ ***p<0.000001, GFP/Nestin+ vs GFP/Tubulin β3+ ***p<0.000001.

(E) Confocal representative images showing the expression of $Nestin^+$ NSCs and $GFAP^+$ astrocytes in spinal cord at 8 weeks after SCI among different treatments. Scale bar (left), 50μm. Scale bar (right), 25μm.

(F) Quantification of relative Nestin expression in the lesion center. n=5 independent animals. Data are presented as mean ± SEM. One-way ANOVA with Tukey HSD post hoc test, Lesion control vs OE-UCHL1-LV **p=0.002,

OE-UCHL1-LV vs rh-UCHL1 *p=0.031, OE-UCHL1-LV vs LDN-57444 ***p=0.00045.

(G) Quantification of relative ratio of cavity areas in the lesion epicenter. n=3 independent animals. Data are presented as mean ± SEM. One-way ANOVA with Tukey HSD post hoc test, UCHL1, Lesion control vs OE-UCHL1-LV ***p=0.000225, Lesion control vs rh-UCHL1 *p=0.042, OE-UCHL1-LV vs rh-UCHL1 *p=0.031, OE-UCHL1-LV vs LDN-57444 ***p=0.000005.

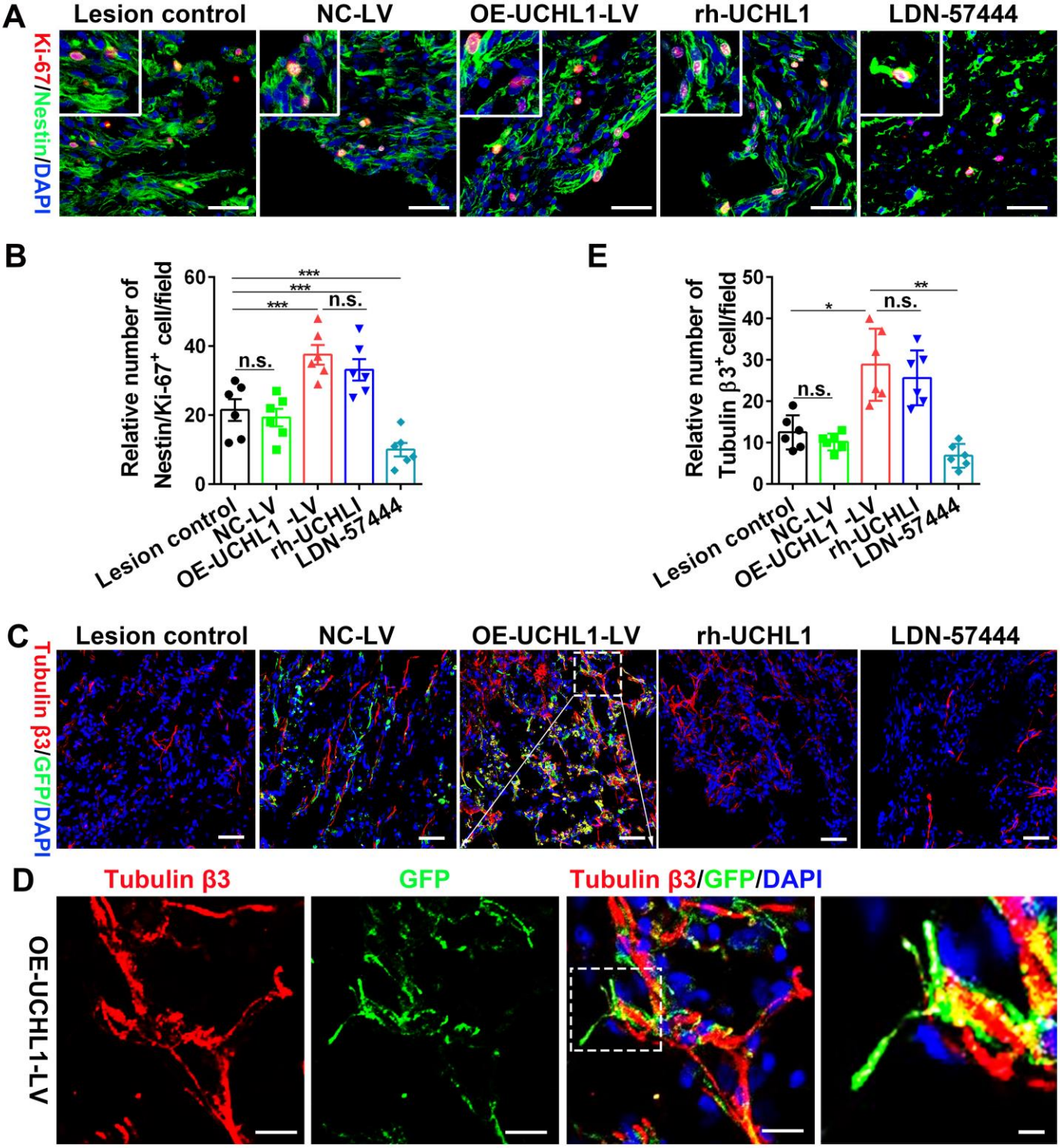

Figure 6 Overexpression of UCHL1 contributed to the proliferation and neuronal differentiation of endogenous NSCs in suit post-SCI

(A) Confocal representative images show the proliferation of NSCs labeled by

Ki-67/Nestin in the lesion core at 7 days after SCI. Scale bar, 20μm.

(B) Quantification of Ki-67/Nestin$^+$ cells in figure A. n=6 independent animals. Data are presented as mean ± SEM. One-way ANOVA with Tukey HSD post hoc test, UCHL1, Lesion control vs OE-UCHL1-LV ***p=0.000006, Lesion control vs rh-UCHL1 ***p=0.000125, OE-UCHL1-LV vs LDN-57444 ***p<0.000001.

(C) Neurons within the lesion center were identified by immunofluorescence staining of Tubulin β3$^+$ at 8 weeks post-SCI. Scale bar, 25μm.

(D) Enlarged images of the boxed region in figure 6C. Scale bar, 20μm.

(E) Quantification of relative Tubulin β3$^+$ neurons in lesion site. n=3 independent animals. Data are presented as mean ± SEM. Kruskal Wallis test with Bonferroni correction, Lesion control vs OE-UCHL1-LV *p=0.035, OE-UCHL1-LV vs LDN-57444 **p=0.003.

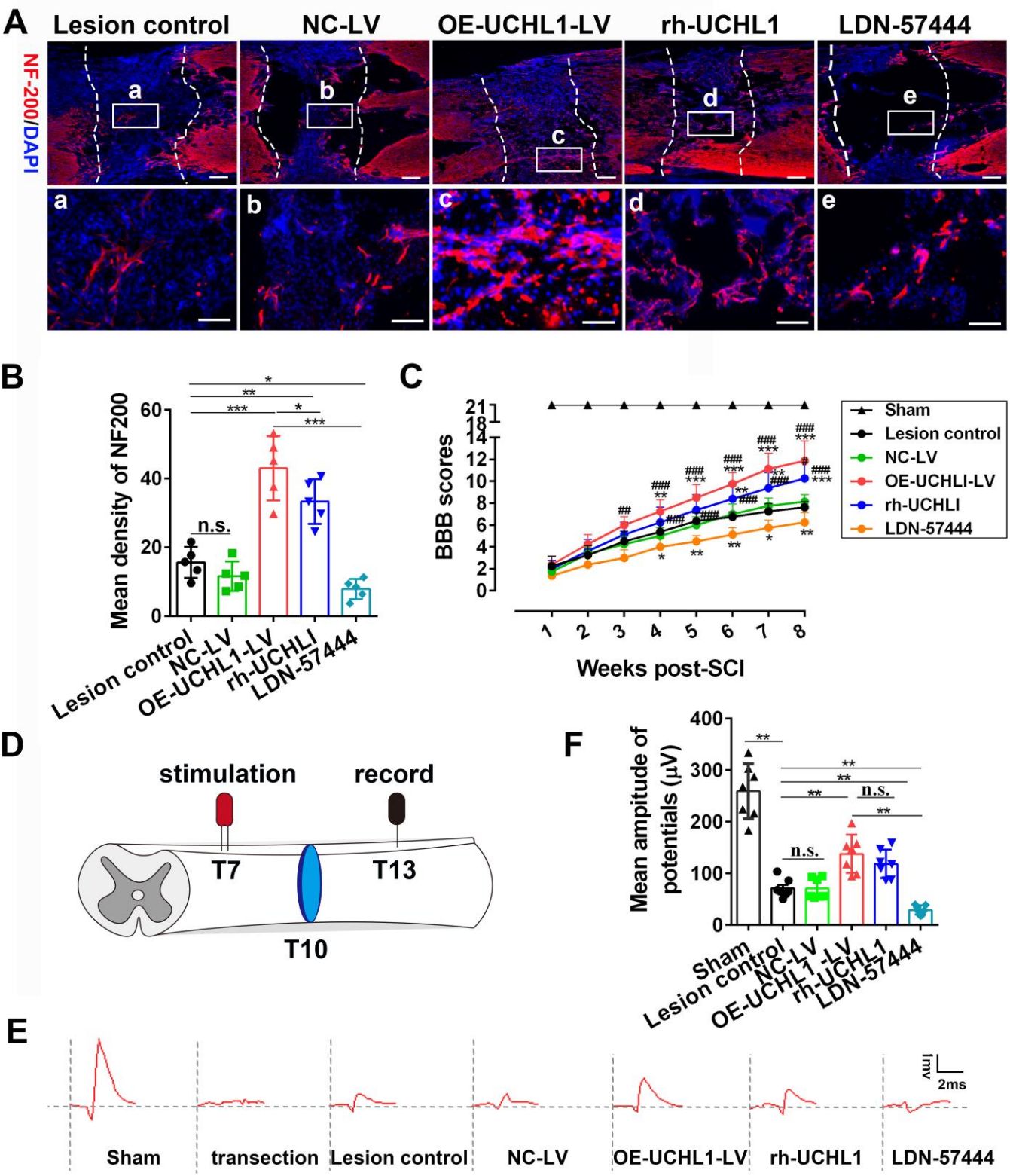

Figure 7 Overexpression of UCHL1 significantly promoted nerve fiber regeneration and conductance, and improved locomotor recovery of SCI

rats

(A) Axonal regeneration across the lesion center was evaluated using immunolabeling of nerve fiber marker NF200. The white dotted line indicated the lesion center. Scale bar (A), 50μm. Scale bar (B), 25μm.

(B) Quantification of relative expression of NF200 in the lesion. n=5 independent animals. Data are presented as mean ± SEM. One-way ANOVA with Tukey HSD post hoc test, UCHL1, Lesion control vs OE-UCHL1-LV ***p=0.000004, Lesion control vs rh-UCHL1 **p=0.001, Lesion control vs LDN-57444 *p=0.042, OE-UCHL1-LV vs rh-UCHL1 *p=0.018, OE-UCHL1-LV vs LDN-57444 ***p<0.000001.

(C) BBB scores of SCI rats among treatments during the 8 weeks post-injury. n=8 independent animals. Data are presented as mean ± SEM. Two-way ANOVA with Tukey post hoc test. 3W, OE-UCHL1-LV vs LDN-57444 ##p=0.002; 4W, Lesion control vs OE-UCHL1-LV **p=0.002, Lesion control vs LDN-57444 *p=0.046, OE-UCHL1-LV vs LDN-57444 ###p<0.000001, rh-UCHL1 vs LDN-57444 ###p=0.00018; 5W, Lesion control vs OE-UCHL1-LV ***p=0.000336, Lesion control vs LDN-57444 **p=0.002, OE-UCHL1-LV vs LDN-57444 ###p<0.000001, rh-UCHL1 vs LDN-57444 ###p=0.00001; 6W, Lesion control vs OE-UCHL1-LV ***p=0.000001, Lesion control vs rh-UCHL1 **p=0.009, Lesion control vs LDN-57444 **p=0.009, OE-UCHL1-LV vs LDN-57444 ###p<0.000001, rh-UCHL1 vs LDN-57444 ###p<0.000001; 7W, Lesion control vs OE-UCHL1-LV ***p=0.000001, Lesion control vs rh-UCHL1

**p=0.001, Lesion control vs LDN-57444 *p=0.037, OE-UCHL1-LV vs LDN-57444 ###p<0.000001, rh-UCHL1 vs LDN-57444 ###p<0.000001; 8W, Lesion control vs OE-UCHL1-LV ***p=0.000001, Lesion control vs rh-UCHL1 ***p=0.000295, Lesion control vs LDN-57444 **p=0.005, OE-UCHL1-LV vs LDN-57444 ###p<0.000001, rh-UCHL1 vs LDN-57444 ###p<0.000001.

(D) Schematic diagram of electrophysiological assay.

(E) Rats were subjected to electrophysiological assay at 8 weeks before perfusion to assess the reestablishment of neural circuit. Representative images of the provoked response were recorded and shown in E.

(F) The amplitude of evoked potential was quantified by the peak-to-peak value. n= 7 independent animals. Data are presented as mean ± SEM. One-way ANOVA with Kruskal Wallis test with Bonferroni correction, Sham vs Lesion control **p=0.006, Lesion control vs OE-UCHL1-LV **p=0.006, Lesion control vs rh-UCHL1 **p=0.002, Lesion control vs LDN-57444 **p=0.005, OE-UCHL1-LV vs LDN-57444 **p=0.002.

See also Extended Data Figure 8 and Figure 9.

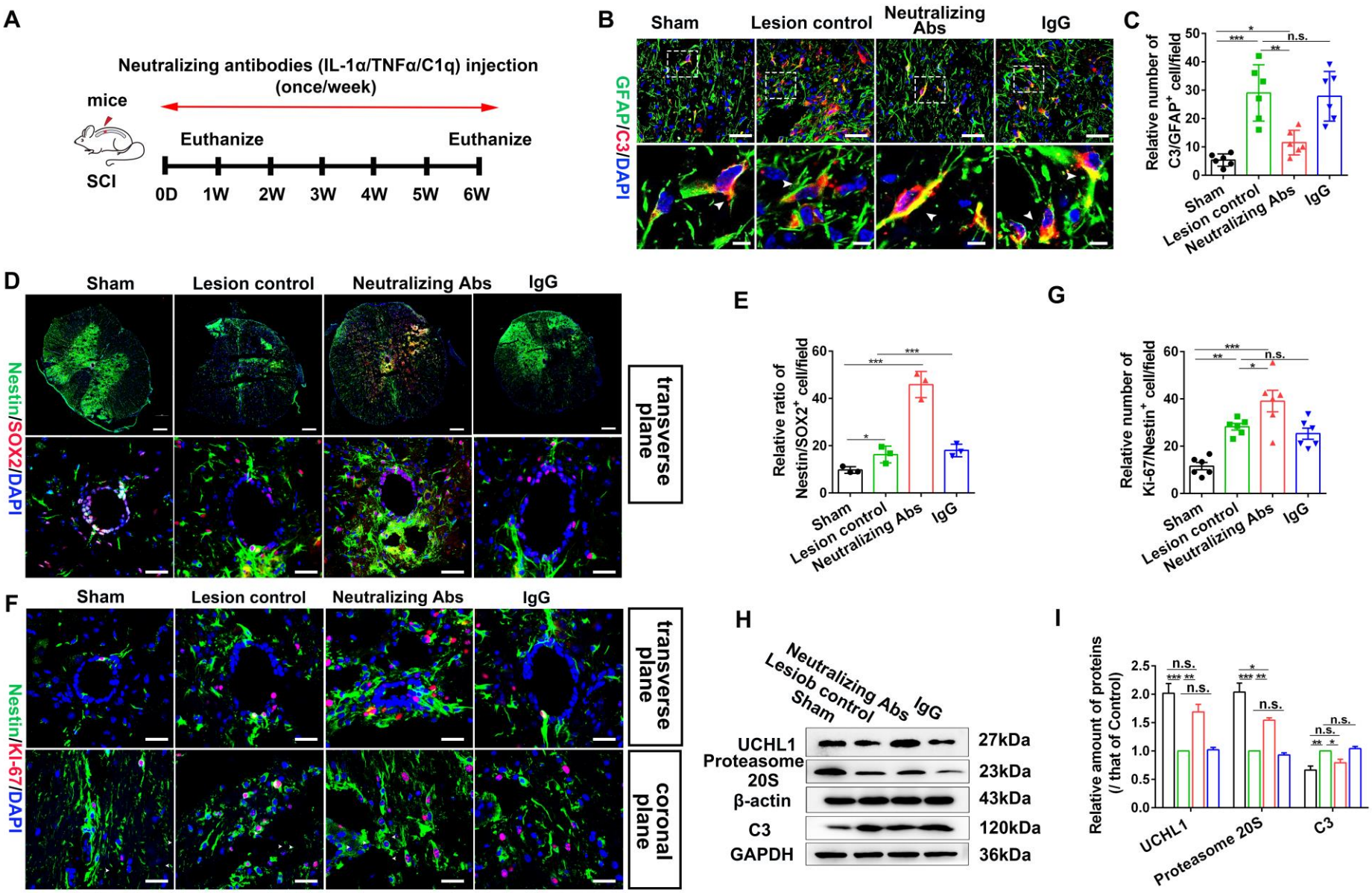
A
Neutralizing antibodies (IL-1α/TNFα/C1q) injection
(once/week)
mice
SCI
Euthanize
Euthanize
0D 1W 2W 3W 4W 5W 6W
B
Sham
Lesion control
Neutralizing Abs
IgG
GFAP/C3/DAPI
C
Relative number of C3/GFAP+ cell/field
Sham
Lesion control
Neutralizing Abs
IgG
D
Sham
Lesion control
Neutralizing Abs
IgG
Nestin/SOX2/DAPI
transverse plane
E
Relative ratio of Nestin/SOX2+ cell/field
Sham
Lesion control
Neutralizing Abs
IgG
G
Relative number of Ki-67/Nestin+ cell/field
Sham
Lesion control
Neutralizing Abs
IgG
F
Sham
Lesion control
Neutralizing Abs
IgG
Nestin/KI-67/DAPI
transverse plane
coronal plane
H
Sham
Lesiob control
Neutralizing Abs
IgG
UCHL1
Proteasome 20S
β-actin
C3
GAPDH
27kDa
23kDa
43kDa
120kDa
36kDa
I
Relative amount of proteins (/ that of Control)
UCHL1
Proteasome 20S
C3

1342

Figure 8 Blockade of A1 astrocytes using neutralizing antibodies effectively enhanced endogenous NSCs proliferation by disinhibition of UCHL1 and UPS activity in SCI mice

(A) Schematic diagram of BALB/C mice underwent complete SCI and treated with triple neutralizing antibodies. SCI mice were administrated with neutralizing antibodies IL-1α/TNFα/C1q or the IgG isotype control by intraperitoneally injection weekly.

(B) Representative images showing the activation of A1 astrocytes (C3/GFAP^{+}) detected by immunofluorescence assay at 7 days post-SCI. Administration of neutralizing antibodies significantly blocked induction of A1 astrocytes after SCI. Enlarged images of the boxed region are shown in the bottom panels. Scale bar (upper), 20μm. Scale bar (down), 10μm.

(C) Quantification of C3^{+} A1 astrocytes in the lesion site at 7 days post-SCI. n=6 independent animals. Data are presented as mean ± SEM. One-way ANOVA with Tukey HSD post hoc test, Sham vs Lesion control ***p=0.000058, Lesion control vs Neutralizing Abs **p=0.002.

(D) Confocal representative photographs of transverse sections of spinal cord showing the mobilization of Nestin/SOX2^{+} endogenous NSCs around the central canal after A1 astrocytes inhibition at 7 days post-SCI. Scale bar (upper), 25μm. Scale bar

(below), 20μm.

(E) Quantification of Nestin/SOX2^{+} NSCs in different groups from transverse sections of spinal cord. n=3 independent animals. Data are presented as mean ± SEM. One-way ANOVA with Tukey HSD post hoc test, Sham vs Lesion control *p=0.048, Sham vs Neutralizing Abs ***p=0.000009, Lesion control vs Neutralizing Abs ***p=0.0004.

(F) Proliferation of NSCs around the central canal (tranverse plane) and in the lesion center (coronal plane) was evaluated by the detection of Ki-67^{+} NSCs via immunofluorescence assay. Scale bar (upper), 20μm.

(G) The relative number of Ki-67/Nestin^{+} cells were counted. n=6 independent animals. Data are presented as mean ± SEM. One-way ANOVA with Tukey HSD post hoc test, Sham vs Lesion control **p=0.002, Sham vs Neutralizing Abs ***p=0.000005, Lesion control vs Neutralizing Abs *p=0.012.

(H-I) Western blotting assay of spinal lysate from SCI mice treated with neutralizing antibodies or IgG isotype control. Representative immunoblot images and quantification of the relative enrichment of proteins were revealed in H and I. n=3 independent animals. (I) n=3 independent animals. Data are presented as mean ± SEM. One-way ANOVA with Tukey HSD post hoc test. UCHL1, Sham vs Lesion control ***p=0.000798, Lesion control vs Neutralizing Abs **p=0.009; Proteasome 20S, Sham vs Lesion control ***p=0.000097, Lesion control vs Neutralizing Abs **p=0.008, Lesion control vs Neutralizing Abs *p=0.012; C3, Sham vs Lesion control **p=0.007, Lesion control vs

Neutralizing Abs *p=0.033.

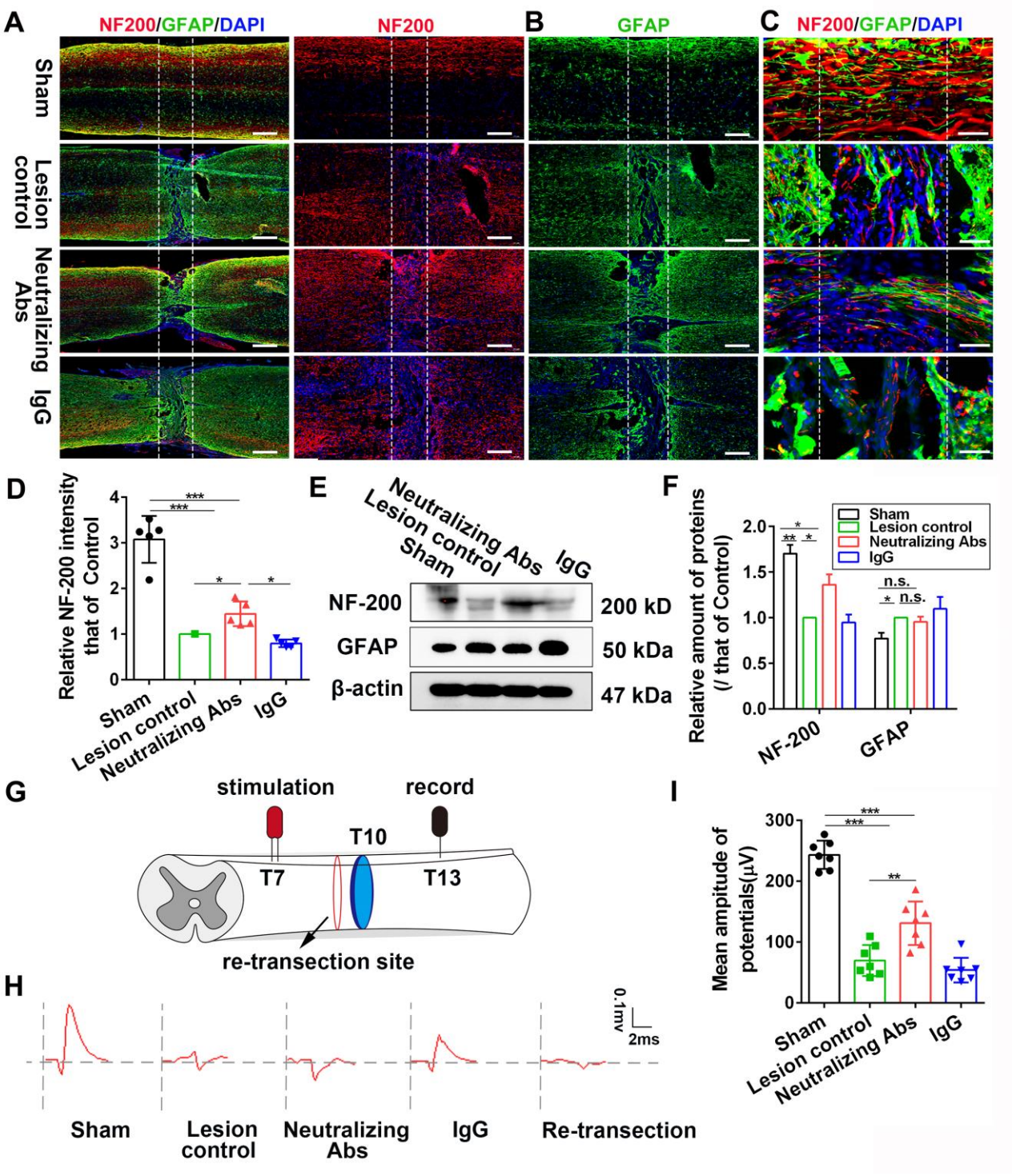

Figure 9 Inhibition of A1 astrocytes formation significantly contributed to nerve regeneration across lesion center, improved neural circuitry and

motor functional recovery in SCI mice

(A-C) Fluorescent assay showed the regenerative axons labeled by NF-200 and astrocytes glial formation in the lesion location at 6-week post-SCI among different treatments. Blockade of A1 astrocytes mediated glial scar remodel (B) and formed a bridge to guide the well-aligned regeneration of axons across through the lesion center (C). The white dotted line indicated the lesion center. Scale bar (A), 100μm. Scale bar (B), 50μm. Scale bar (C), 10μm.

(D) The relative amount of NF-200^{+} nerve fibers within the lesion epicenter were quantified. n=5 independent animals. Data are presented as mean ± SEM. One-way ANOVA with Tukey HSD post hoc test, Sham vs Lesion control ***p<0.000001, Sham vs Neutralizing Abs ***p<0.000001, Lesion control vs Neutralizing Abs *p=0.03, Neutralizing Abs vs IgG *p=0.015.

(E-F) Western blot analysis was conducted to measure the expression of NF-200 and myelin-related protein MBP at 6-week post-SCI in animals. Representative immunoblot images and quantification of proteins were show in E and F. (F) n=3 independent animals. Data are presented as mean ± SEM. One-way ANOVA with Tukey HSD post hoc test, NF-200, Sham vs Lesion control **p=0.002, Sham vs Neutralizing Abs *p=0.024, Lesion control vs Neutralizing Abs *p=0.019; GFAP, Sham vs Lesion control *p=0.045.

(G) Schematic diagram of electrophysiological assay in mice.

(H) Representative images of evoked potentials in SCI mice at 6 weeks after treatment.

(I) The amplitude of individual potential was quantified upon the peak-to-peak value. n=7 independent animals. Data are presented as mean ± SEM. One-way ANOVA with Tukey HSD post hoc test, Sham vs Lesion control ***p<0.000001, Sham vs Neutralizing Abs ***p<0.000001, Lesion control vs Neutralizing Abs **p=0.001.

See also Extended Data Figure 10 and Figure 11.

Extended Data

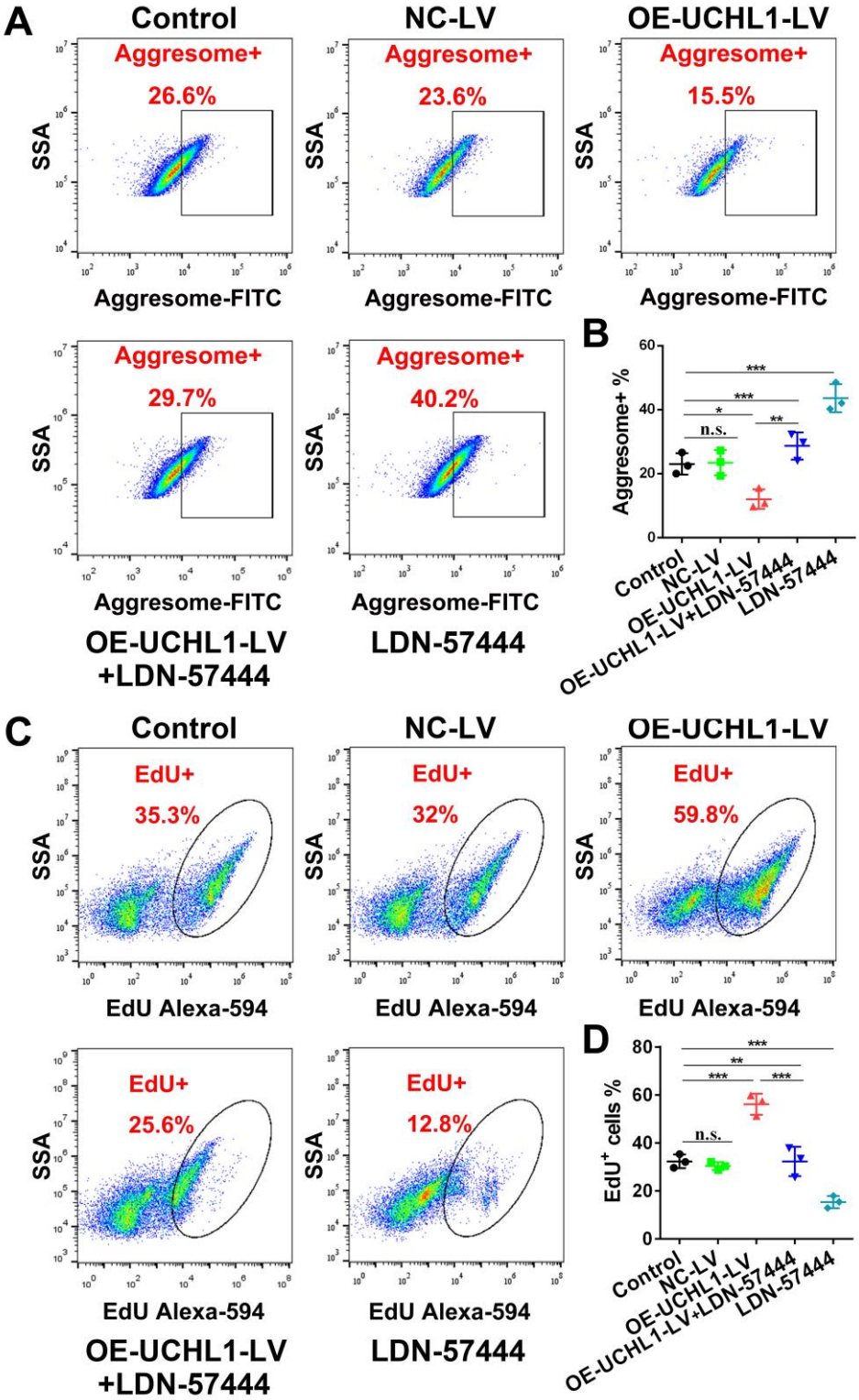

Extended Data Figure 1 Flow cytometry analysis of Protein aggregation

accumulation and proliferation of NSCs treated with NC-LV, OE-UCHL1-LV, OE-UCHL1-LV+LDN-57444 and LDN-57444

(A-B) Flow cytometry analysis (A) and quantification (B) of protein aggregates (aggresome+) in NSCs. (B) n=3 biological replicates. Data are presented as mean ± SEM. One-way ANOVA with Tukey HSD post hoc test, Control vs OE-UCHL1-LV *p=0.035, OE-UCHL1-LV vs OE-UCHL1-LV+LDN-57444 **p=0.002435, Control vs LDN-57444 ***p=0.000472, OE-UCHL1-LV vs LDN-57444 ***p=0.000011.

(C-D) The proliferating NSCs (EdU^+) in different treatments were detected by flow cytometry assay (C) and quantified (D). (D) n=3 biological replicates. Data are presented as mean ± SEM. One-way ANOVA with Tukey HSD post hoc test, Control vs OE-UCHL1-LV ***p=0.000146, OE-UCHL1-LV vs OE-UCHL1-LV+LDN-57444 ***p=0.000114, Control vs LDN-57444 **p=0.002281, OE-UCHL1-LV vs LDN-57444 ***p=0.000001.

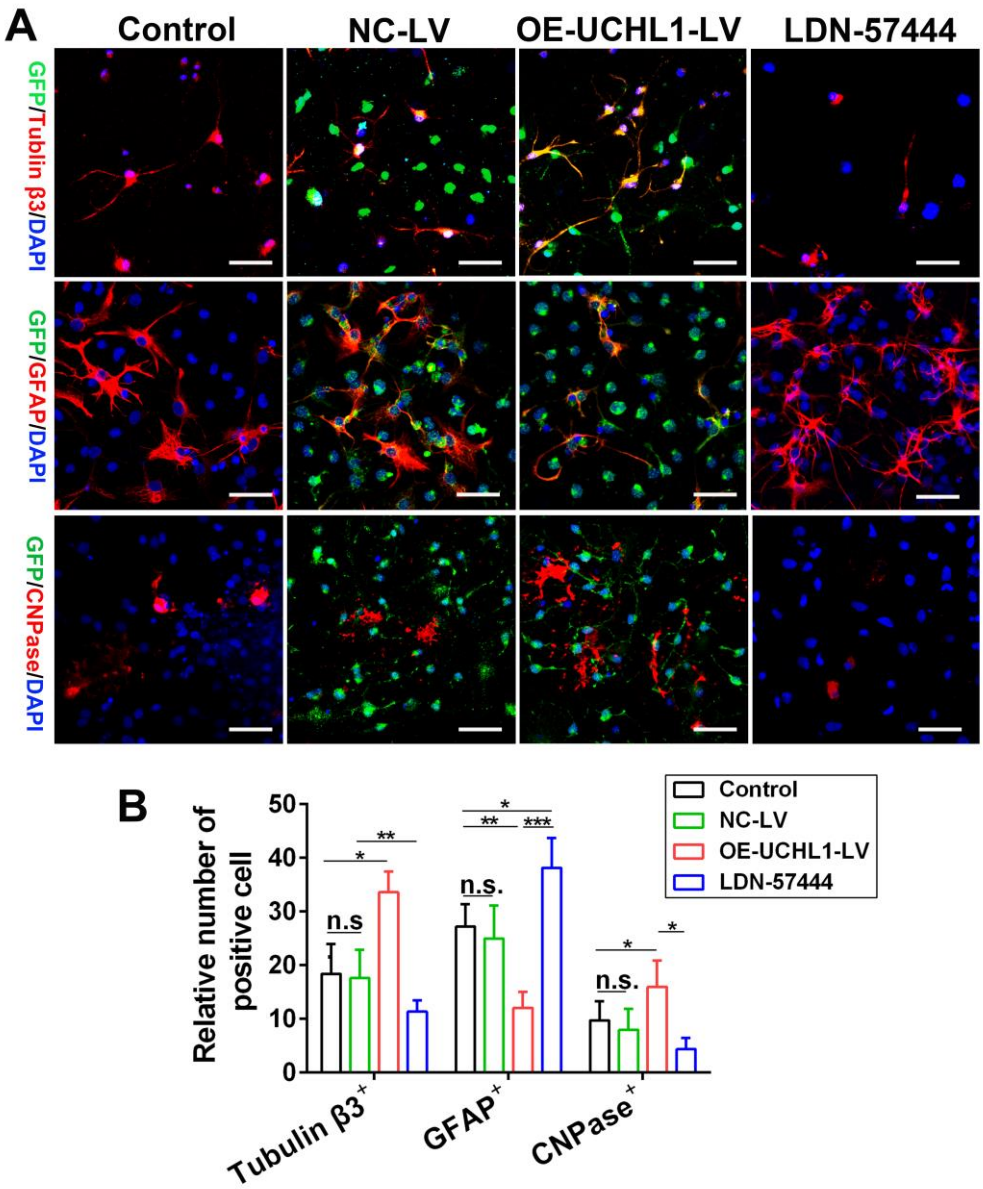

Extended Data Figure 2 Upregulation of UCHL1 promoted neuronal differentiation of NSCs in vitro

(A) Representative images showing the differentiation of NSCs treated with GFP-NC-LV, GFP-OE-UCHL1-LV or LDN-57444 for 7 days. Scale bar, 100μm. (B) Quantification of the relative ratio of differentiated neurons (Tubulin β3^{+}), astrocytes (GFAP^{+}) and oligodendrocyte (CNPase^{+}). n=3 biological replicates. Data are presented as mean ± SEM. One-way ANOVA with Tukey HSD post

hoc test. Tubulin β3^{+} cell, Control vs OE-UCHL1-LV *p=0.012, OE-UCHL1-LV vs LDN-57444 **p=0.001; GFAP^{+} cell, Control vs OE-UCHL1-LV **p=0.021, Control vs LDN-57444 *p=0.046, OE-UCHL1-LV vs LDN-57444 ***p=0.000792; CNPase^{+} cell, Control vs OE-UCHL1-LV *p=0.031, OE-UCHL1-LV vs LDN-57444 *p=0.021.

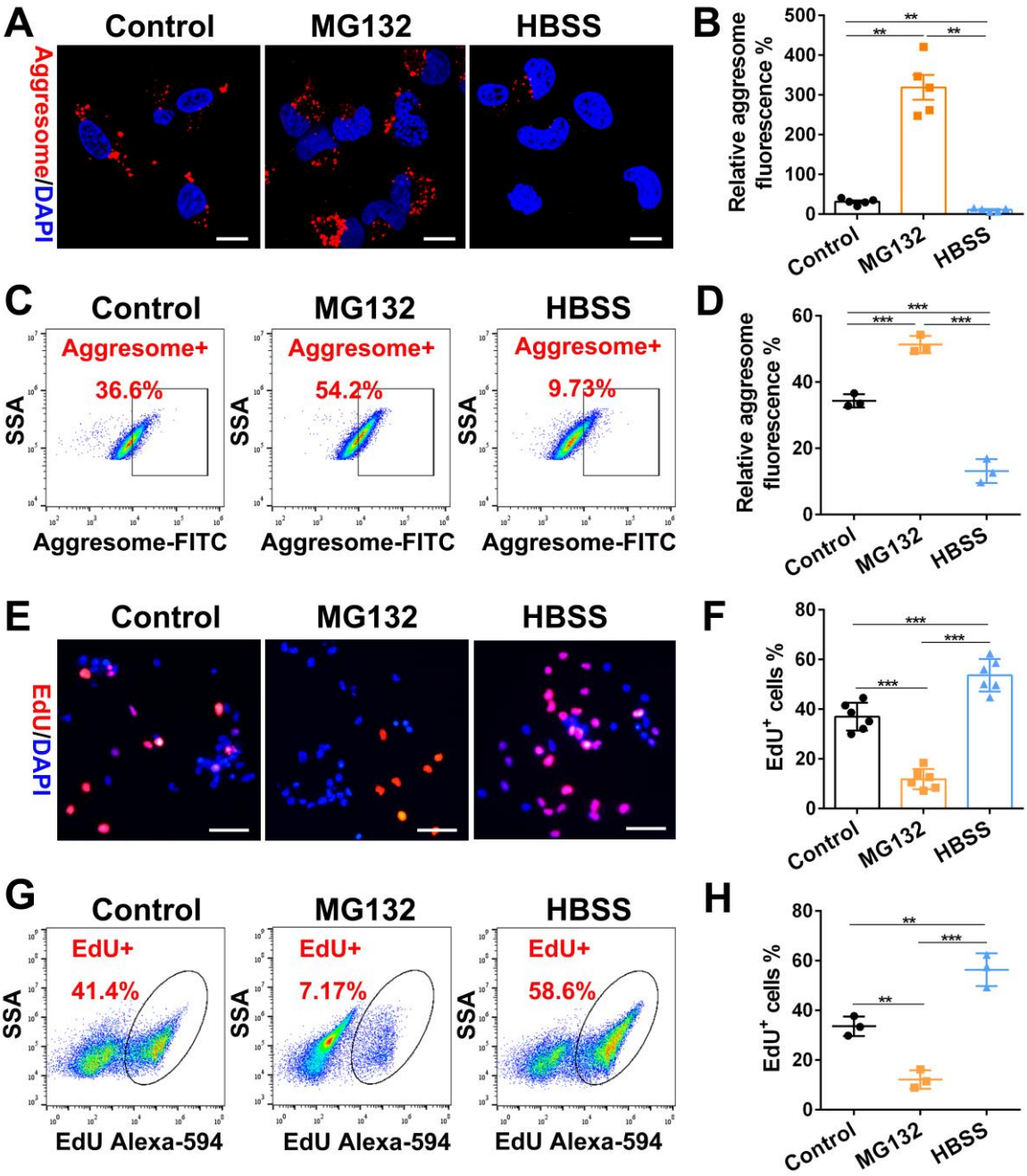

Extended Data Figure 3 Protein aggregates in NSCs made an inhibitory effect on cell proliferation directly

(A) Confocal representative images showing protein aggregates labeled by aggresome dye (red) in NSCs treated with MG132 (proteasome inhibitor) or incubated with HBSS for 3h prior to be transferred into the basal medium. Scale bar, 10μm.

(B) Quantification of protein aggregates accumulated in NSCs. n=5 biological replicates. Data are presented as mean ± SEM. One-way ANOVA with Tamhane T2 post hoc test, Control vs MG132 **p=0.002, Control vs HBSS **p=0.005, MG132 vs HBSS **p=0.002.

(C-D) Flow cytometry analysis (C) and quantification (D) of protein aggregates in NSCs treated with MG132 or HBSS. (D) n=3 biological replicates. Data are presented as mean ± SEM. One-way ANOVA with Tukey HSD post hoc test, Control vs MG132 ***p=0.000756, Control vs HBSS ***p=0.000222, MG132 vs HBSS ***p=0.000007.

(E-H) Fluorescent staining (E-F) and flow cytometry analysis (G-H) show the proliferation of NSCs treated with MG132 or HBSS for 12h. Scale bar (E), 25μm. (F) n=6 biological replicates. Data are presented as mean ± SEM. One-way ANOVA with Tukey HSD post hoc test, Control vs MG132 ***p=0.000003, Control vs HBSS ***p=0.00028, MG132 vs HBSS ***p<0.000001. (H) n=3 biological replicates. Data are presented as mean ± SEM. One-way ANOVA with Tukey HSD post hoc test, Control vs MG132 **p=0.004, Control vs HBSS **p=0.003, MG132 vs HBSS ***p=0.000086.

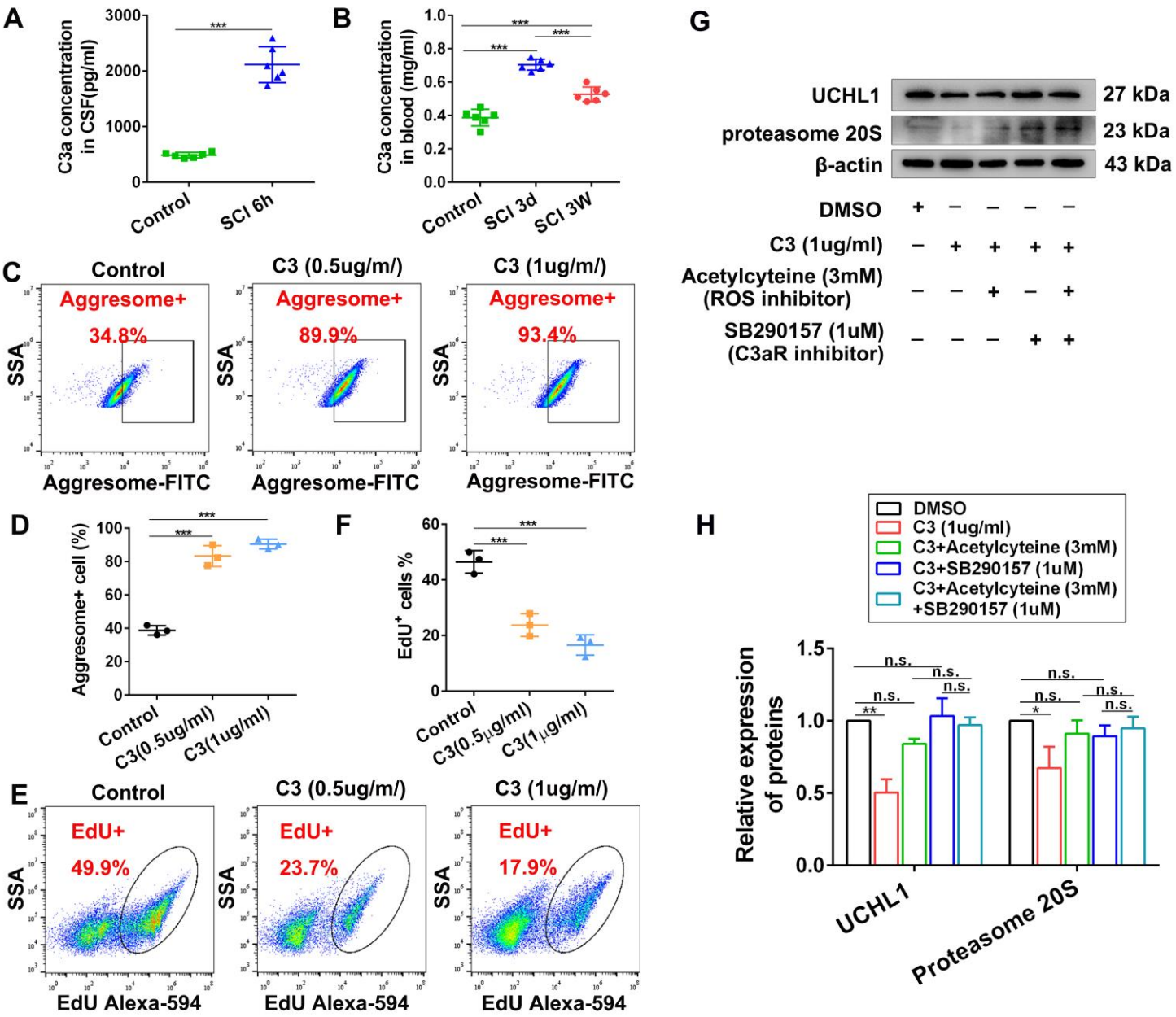

Extended Data Figure 4 Flow cytometry analysis of protein aggresome accumulation and proliferation of NSCs treated with C3

(A-B) The level of C3 in CSF (A) and (B) blood of SCI rats were detected by ELISA analysis. (A) n=6 biological replicates. Data are presented as mean ± SEM. Two-tailed unpaired Student's t-test, ***p=0.000047. (B) n=6 biological replicates. Data are presented as mean ± SEM. One-way ANOVA with Tukey

HSD post hoc test, Control vs SCI 3d ***p<0.000001, Control vs SCI 3W ***p=0.000119, SCI 3d vs SCI 3W ***p=0.000009.

(C-D) Flow cytometry analysis (C) and quantification (D) of accumulated protein aggregates (aggresome^{+}) in NSCs treated with C3 for 24h. (D) n=3 biological replicates. Data are presented as mean ± SEM. One-way ANOVA with Tukey HSD post hoc test, Control vs C3 (0.5 ug/ml) ***p=0.000036, Control vs C3 (1 ug/ml) ***p=0.000015.

(E-F) The activation of NSCs after treated with C3 was evaluated (E) and (F) quantified by EdU^{+} NSCs through Flow cytometry analysis. (F) n=3 biological replicates. Data are presented as mean ± SEM. One-way ANOVA with Tukey HSD post hoc test, Control vs C3 (0.5 ug/ml) ***p=0.000982, Control vs C3 (1 ug/ml) ***p=0.000216.

(G) Western blot analysis of NSCs treated with ROS inhibitor and C3aR inhibitor was conducted with indicated antibodies.

(H) Quantification of relative protein expression in NSCs treated with ROS inhibitor and C3aR inhibitor. n=3 biological replicates. Data are presented as mean ± SEM. One-way ANOVA with Tukey HSD post hoc test. UCHL1, DMSO vs C3 (1 ug/ml) **p=0.006; Proteasome 20S, DMSO vs C3 (1 ug/ml) *p=0.031.

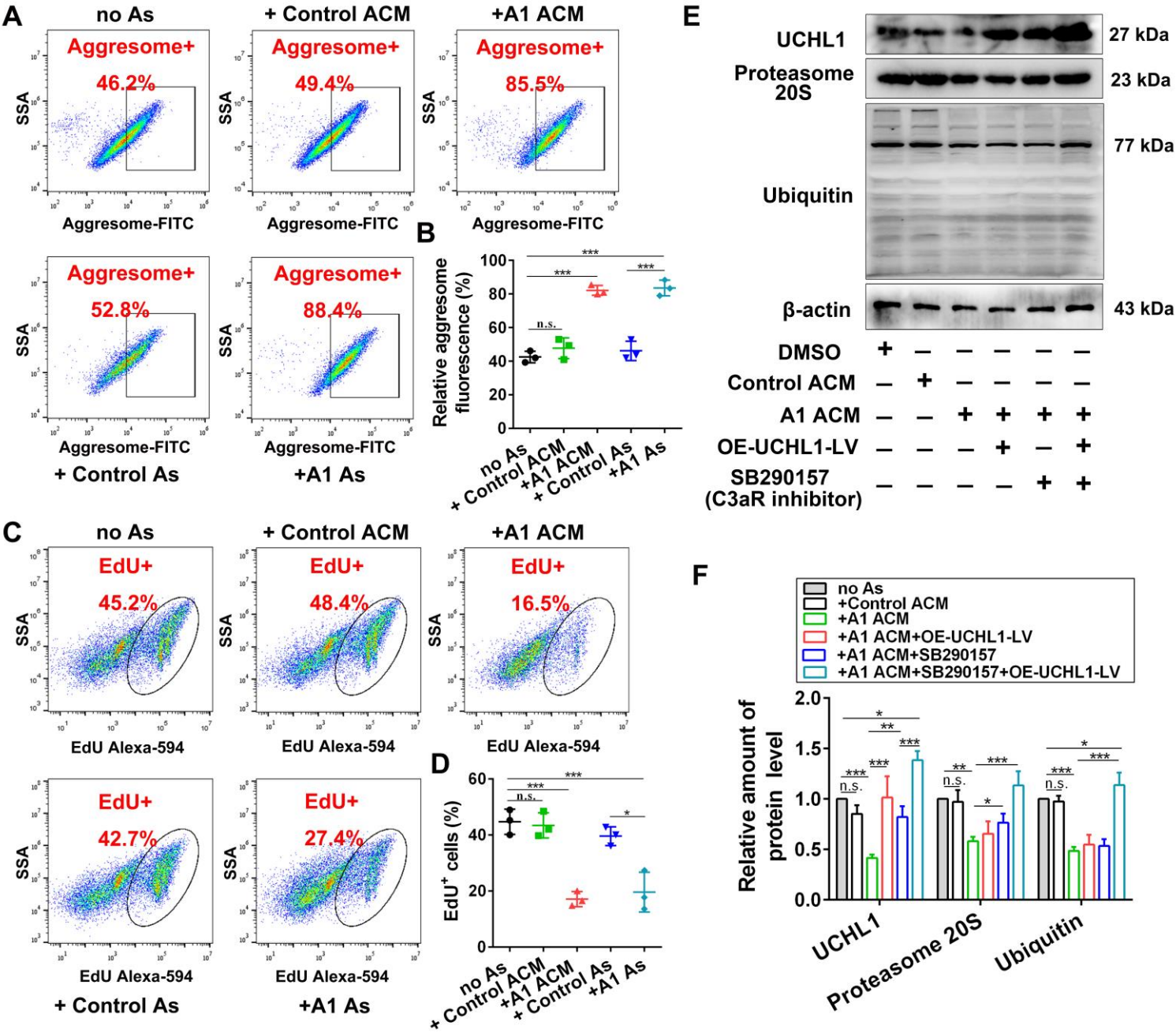

Extended Data Figure 5 Detection of protein aggregates and cell activation in NSCs co-cultured with control or A1 astrocytes by flow cytometry assay

(A-B) Flow cytometry analysis (A) and quantification (B) of accumulated protein aggregates (aggresome^{+}) in NSCs co-cultured with astrocytes 24h. (B)

n=3 biological replicates. Data are presented as mean ± SEM. One-way ANOVA with Tukey HSD post hoc test, no As vs +A1 ACM ***p=0.000001, no As vs +A1 As ***p=0.000001, +Control AS vs +A1 As ***p=0.000002.

(C-D) The activation of NSCs after treated with C3 was evaluated (C) and quantified (D) by EdU^+ NSCs by Flow cytometry assay. (D) n=3 biological replicates. Data are presented as mean ± SEM. One-way ANOVA with Tukey HSD post hoc test, no As vs +A1 ACM ***p=0.000023, no As vs +A1 As ***p=0.00006, +Control AS vs +A1 As ***p=0.00037.

(E-F) Western blot analysis of NSCs treated with OE-UCHL1-LV and C3aR inhibitor in the A1 astrocytes conditioned medium was conducted with indicated antibodies. Representative immunoblot images and quantification of relative protein level was illustrated in E and F. (F) n=3 biological replicates. Data are presented as mean ± SEM. One-way ANOVA with Tukey HSD post hoc test, UCHL1, DMSO vs A1 ACM ***p=0.000326, DMSO vs A1 ACM+SB290157+OE-UCHL1-LV *p=0.01, A1 ACM vs A1 ACM +OE-UCHL1-LV ***p=0.000263, A1 ACM vs A1 ACM+SB290157 **p=0.007, A1 ACM vs A1 ACM+SB290157+OE-UCHL1-LV *** p=0.000002. Proteasome 20S, DMSO vs A1 ACM **p=0.003, A1 ACM vs A1 ACM+SB290157+OE-UCHL1-LV ***p=0.00022, A1 ACM+SB290157 vs A1 ACM+SB290157+OE-UCHL1-LV ***p=0.000805. Ubiquitin, DMSO vs A1 ACM ***p=0.000027, A1 ACM vs A1 ACM+SB290157+OE-UCHL1-LV *** p=0.000002.

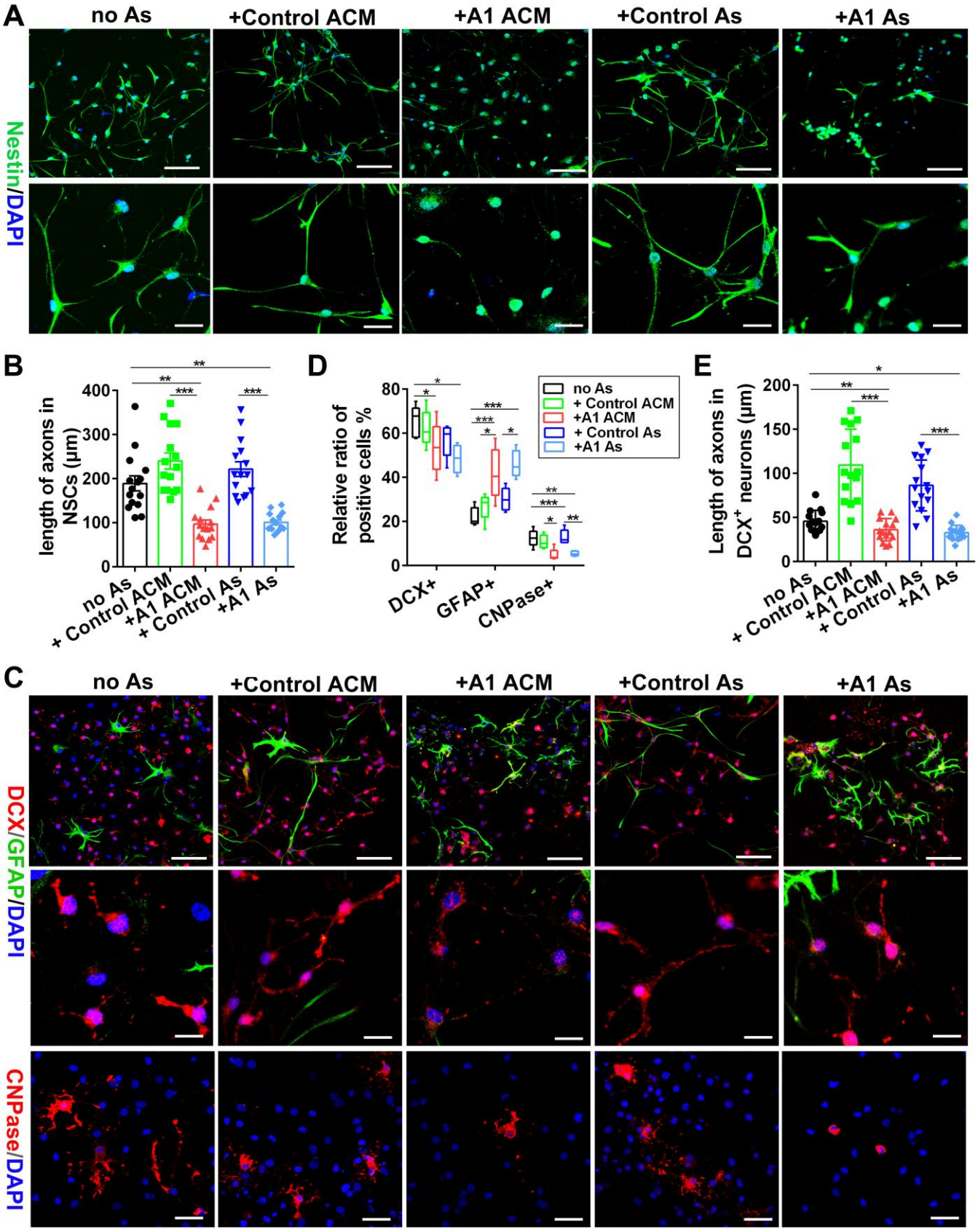

1569

1570 **Extended Data Figure 6 A1 astrocytes may suppress process extension**

and neuron generation of NSCs

(A) NSCs were underwent adherent co-culture either with the control or A1 ACM and control or A1 astrocytes for 24h, then subjected to fluorescent staining with Nestin. Representative images show A1 astrocytes and A1 ACM inhibited the axonal out-extending of NSCs. Scale bar (upper), 50μm. Scale bar (down), 20μm.

(B) The length of axons in NSCs co-cultured either astrocytes or ACM was quantified in different groups. n=3 biological replicates. Data are presented as mean ± SEM. Kruskal Wallis test with Bonferroni correction, no As vs +A1 ACM **p=0.003, no As vs +A1 As **p=0.004, +Control ACM vs A1 ACM ***p<0.0001, +Control AS vs +A1 As ***p<0.0001.

(C) NSCs were co-cultured either with the control or A1 ACM and astrocytes to induce differentiation for 7 days. The differentiated neurons, astrocytes and oligodendrocytes were identified individually using immunofluorescence assay by indicated markers. Scale bar (the upper line), 50μm. Scale bar (the below two lines), 20μm.

(D) The percentage of DCX^+ neurons, $GFAP^+$ astrocytes, MBP^+ oligodendrocytes generated from NSCs were quantified. n=3 biological replicates. Data are presented as mean ± SEM. One-way ANOVA with Tukey HSD post hoc test. DCX+ cell, no As vs +A1 ACM *p=0.033, no As vs +A1 As *p=0.03; GFAP+ cell, no As vs +A1 ACM **p=0.002, no As vs +A1 As ***p=0.000275, +Control ACM vs A1 ACM *p=0.025, +Control AS vs +A1 As

*p=0.015; CNPase+ cell, no As vs +A1 ACM **p=0.004, no As vs +A1 As **p=0.009, +Control ACM vs A1 ACM *p=0.029, +Control AS vs +A1 As **p=0.005.

(E) The length of DCX^+ neuronal process was measured and quantified. n=3 biological replicates. Data are presented as mean ± SEM. Kruskal Wallis test with Bonferroni correction, no As vs +A1 ACM **p=0.003, no As vs +A1 As *p=0.043, +Control ACM vs A1 ACM ***p<0.0001, +Control AS vs +A1 As ***p<0.0001.

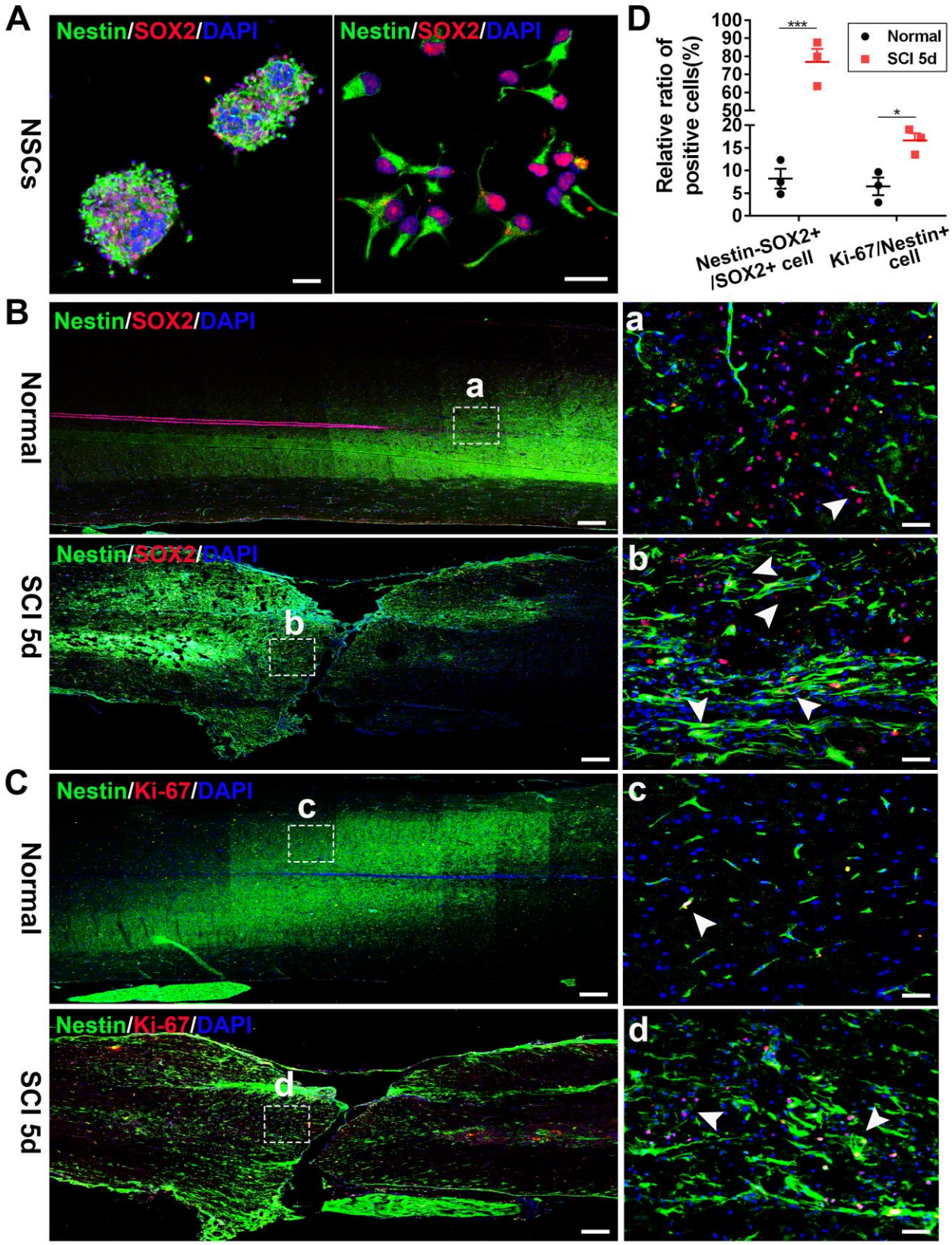

1613 **Extended Data Figure 7 Nestin⁺ endogenous NSCs were activated after**

1614 **SCI in rats.**

(A) NSCs extracted from the fetal brain of SD rats were identified by the double-labeling of Nestin and SOX2 in vitro. All most NSCs were Nestin/SOX2^{+} cells. Scale bar (left), 25μm. Scale bar (right), 20μm.

(B) Activation of Nestin/SOX2^{+} cells at the acute phase of SCI rats. Nestin/SOX2^{+} cells were largely activated around the center lesion post-SCI. a and b were the enlarged images in the white dotted box. The white arrows indicated Nestin/SOX2^{+} cells. Scale bar, 25μm.

(C) Validation of the proliferation ability of Nestin^{+} cells at 5-day after SCI. c were the enlarged images in the white dotted box. The white arrows indicated Ki-67/Nestin^{+} cells. Scale bar, 25μm.

(D) The relative ratio of Nestin/SOX2^{+} cells to that of Nestin^{+} cells were quantified. n=3 independent animals. Data are presented as mean ± SEM. Two-tailed unpaired Student's t-test, ***p=0.000764, *p=0.016.

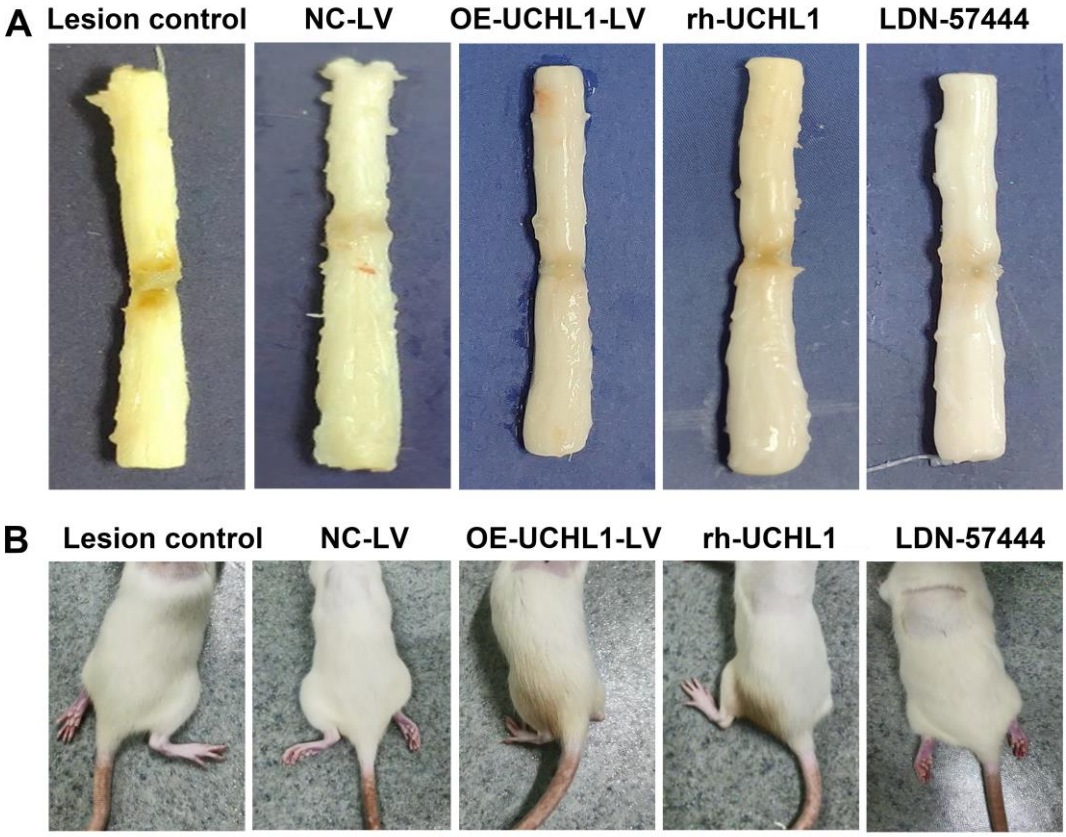

Extended Data Figure 8 Overexpression of UCHL1 preserve tissue integrity and improved locomotor performance in SCI rats

(A) Representative gross specimen of spinal cord encompassing the lesion epicenter at 8 weeks after SCI in different groups.

(B) Representative images showing the functional behavior of hindlimbs in SCI rats at 8 weeks post-injury.

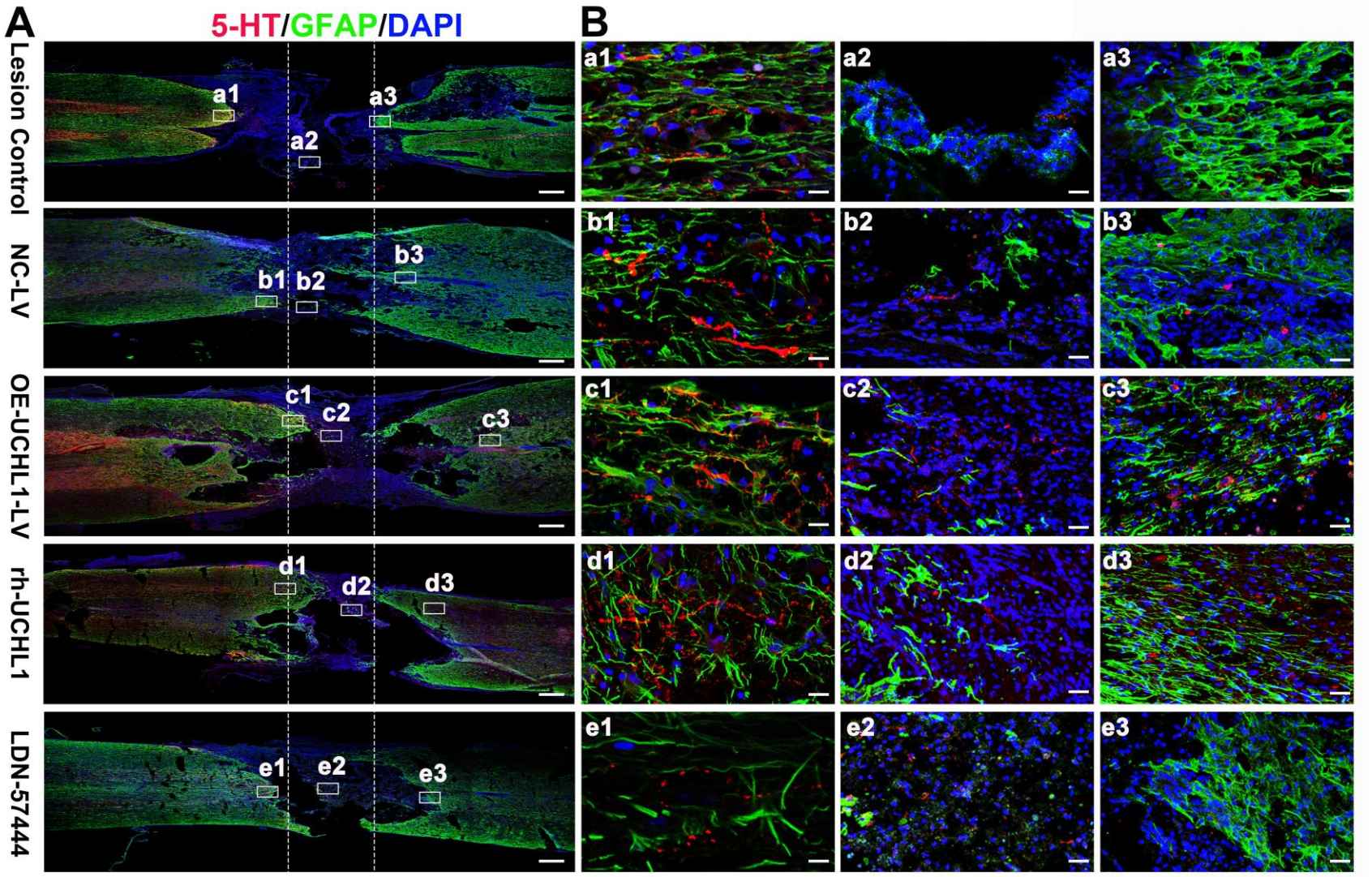
A
5-HT/GFAP/DAPI
B
Lesion Control
NC-LV
OE-UCHL1-LV
rh-UCHL1
LDN-57444
a1
a2
a3
b1
b2
b3
c1
c2
c3
d1
d2
d3
e1
e2
e3

1650

Extended Data Figure 9 Upregulation of UCHL1 promoted regeneration of 5-HT fibers post-SCI

(A-B) Rats underwent T10 complete SCI and treated with OE-UCHL1-LV, rh-UCHL1 and LDN-57444. The regrowth of serotonergic fibers was evaluated by immunofluorescence assay at 8 weeks post-SCI. Improvement of 5-HT axonal regeneration was observed in rats administrated with OE-UCHL1-LV and rh-UCHL1, compared to the controls. Enlarged views of the box regain were shown in B. The white dotted line indicated the lesion center. Scale bar (A), 50μm. Scale bar (B), 25μm.

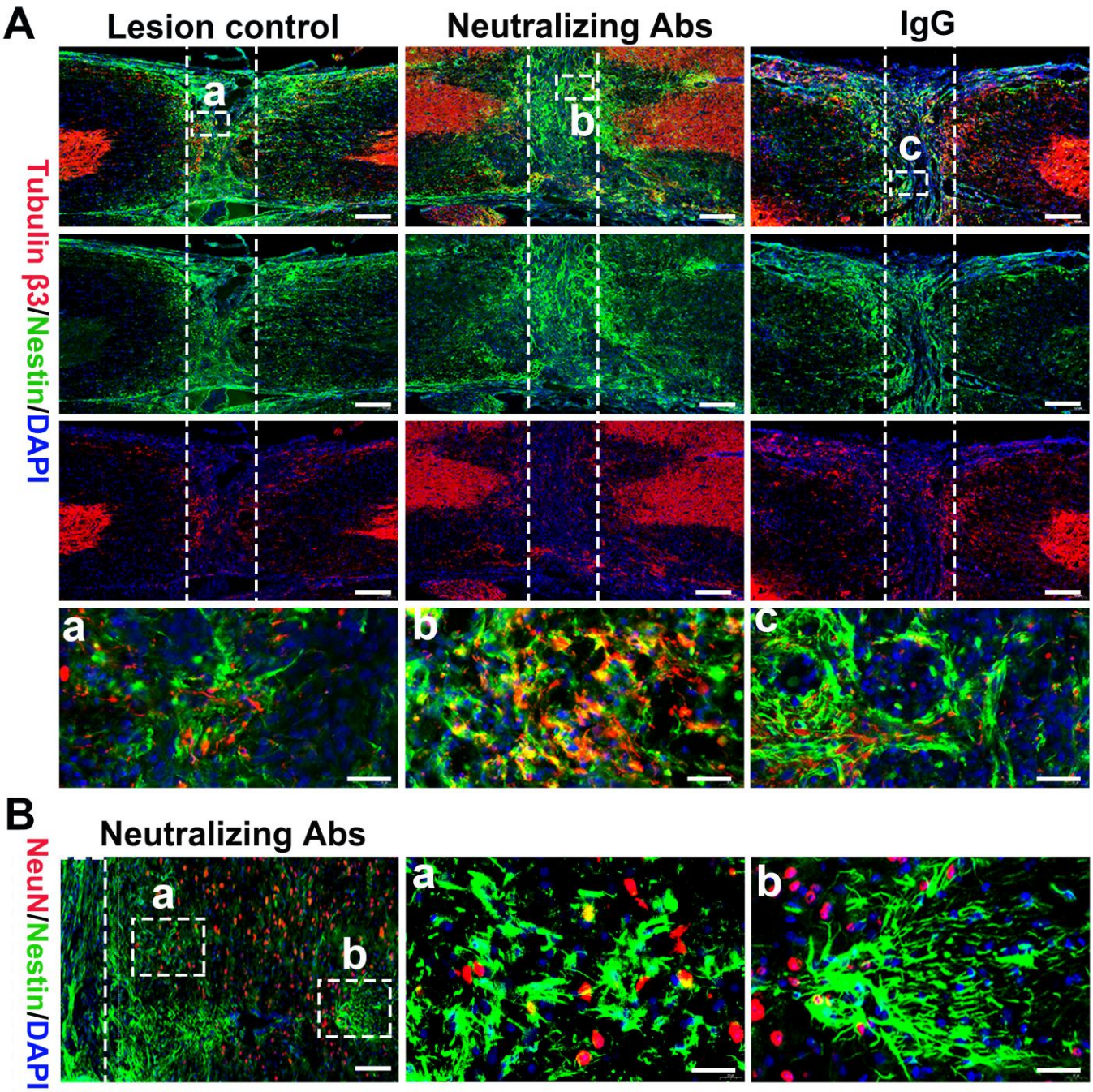

Extended Data Figure 10 Blocking A1 astrocytes polarization facilitated migration of activated NSCs and neuronal generation in SCI mice

(A) Fluorescent staining with Nestin and Tubulin β3 indicated blockade of A1 astrocytes promoted the activating endogenous NSCs' migration into lesion core and generation of new neurons (Tubulin β3/Nestin^{+}) at 5 weeks after SCI. The white dotted line indicated the lesion center. Scale bar (A), 50μm. Scale

bar (a, b, c), 20μm.

(B) Confocal representative photograph showed activating NSCs contacted with $NeuN^+$ mature neurons caudal to the lesion site when A1 astrocytes was inhibited by neutralizing antibodies. The white dotted line indicated the lesion center. Scale bar (left), 50μm. Scale bar (a, b), 20μm.

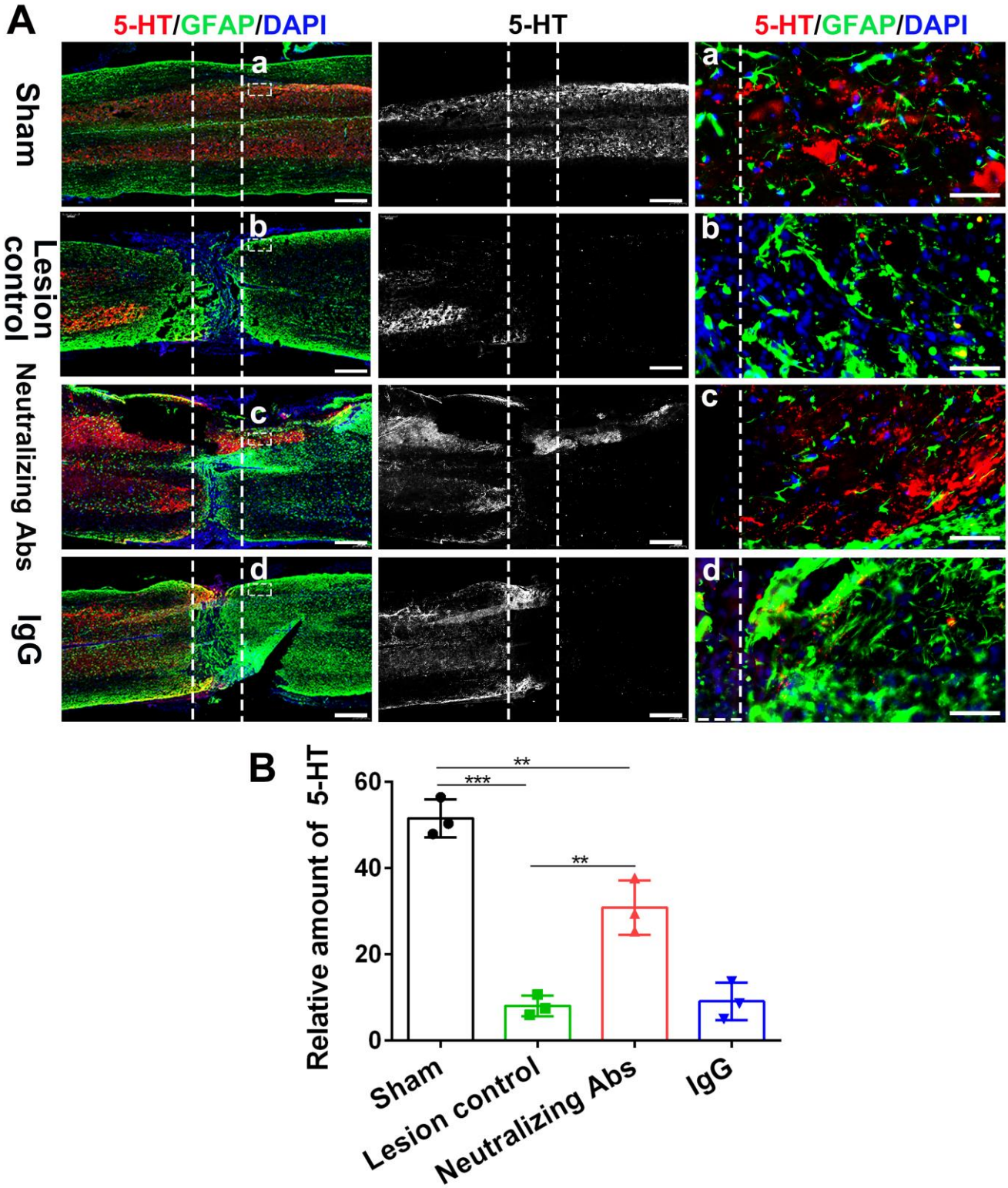

Extended Data Figure 11 Inhibition of A1 astrocytes by neutralizing antibodies facilitated 5-HT axons across through the lesion center in SCI mice

(A) SCI mice were administrated with neutralizing antibodies and its IgG control weekly. Fluorescent staining with 5-HT and GFAP was performed at 6 weeks after SCI. Representative photograph shows the regrowing 5-HT fibers robustly passed through the lesion site with the guidance of modified astrocytes bridge in neutralizing antibodies mice. The white dotted line indicated the lesion center. Scale bar (left), 100μm. Scale bar (a, b, c, d), 10μm.

(B) The relative amount of 5-HT in figure S12A was quantified. n=3 independent animals. Data are presented as mean ± SEM. One-way ANOVA with Tukey HSD post hoc test, Sham vs Lesion control ***p=000012, Sham vs Neutralizing Abs **p=002, Lesion control vs Neutralizing Abs **p=001.

Graphical Abstract

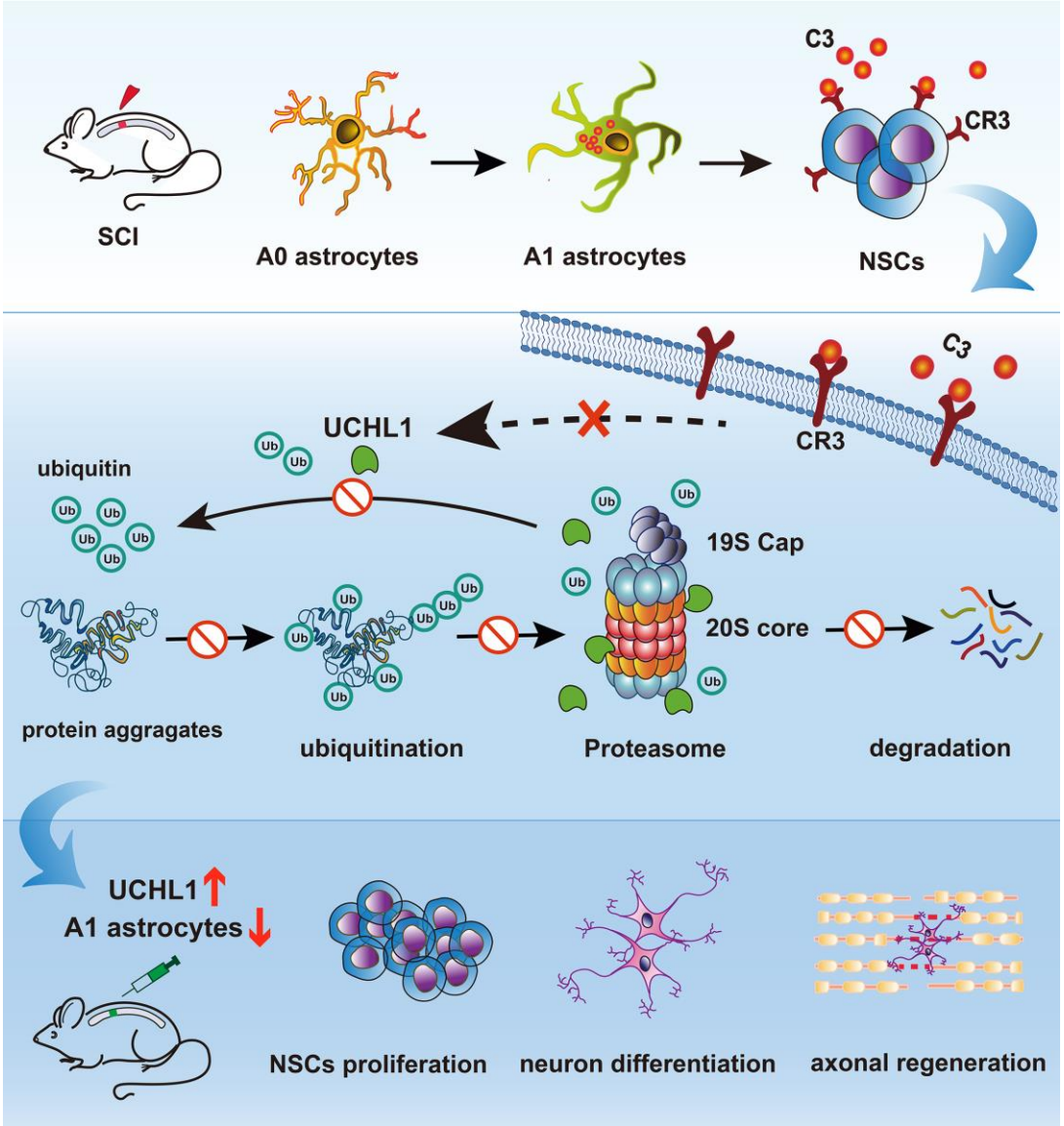

Highlights

- UCHL1 facilitates NSCs activation by clearing intracellular protein aggregates through ubiquitin-proteasome approach
- A1 reactive astrocytes result in down-regulation of UCHL1 to inhibit spinal NSCs activation by C3 after SCI
- Overexpression of UCHL1 or blockade of A1 astrocytes lead to NSCs activation and neurons formation to promote SCI repair via UCHL1-proteasome pathway

Supplementary Tables

Table 1. Primer sequences of genes by qPCR

Gene names	Forward primer (5'-3')	Reverse primer (5'-3')	Length (bp)
UCHL1	TGAAGCAGACCATCGGGAAC	GAGTCATGGGCTGCCTGAAT	190
UCHL3	GGTCAGACTGAGGCACCAAG	CTCATCAGGGTCGCGCTC	195
UCHL5	AGACCTTAGCAGAACACCAGC	CAGCAGTGTACACATGTCCAAAT	119
GAPDH	TGATTCTACCCACGGCAAGTT	TGATGGGTTTCCCATTGATGA	21